

Direct Nanofiltration of Surface Water

Anurag Arun

Technische Universiteit Delft

Direct Nanofiltration of Surface Water

Investigating the fouling and rejection performance of Low MWCO Hollow fiber Nanofiltration Membranes

by

Anurag Arun

to obtain the degree of Master of Science
at the Delft University of Technology,
to be defended publicly on Wednesday December 11, 2019 at 03:00 PM.

Student number: 4716264
Project duration: February 14, 2019 – December 11, 2019
Thesis committee: Prof. dr. ir. S. G. J. Heijman, TU Delft, supervisor
Prof. dr. ir. A. H. Haidari, TU Delft
Prof. dr. ir. L. Rietveld, TU Delft
Prof. dr. ir. H. Spanjers, TU Delft

This thesis is confidential and cannot be made public until December 11, 2021.

An electronic version of this thesis is available at
<http://repository.tudelft.nl/>.

Acknowledgments

I would like to use this opportunity to thank the many people without whom completing this journey would not have been possible.

Firstly, a big thanks to Dr. Bas Heijman for being a supportive and approachable mentor not only for the duration of my research work but also for the rest of my time at TU Delft. I would also like to thank my graduation committee: Dr. Amir Haidari, Dr. Henri Spanjers and Dr. Luuk Rietveld for their valuable feedback and advise. I would also like to specially thank Edoardo Bologna who helped me kickstart this project in good time and David Salas who was always available for questions. With Edoardo's help, I was able to overcome the several teething problems we faced during the commencement of the research. Also a special thanks to the entire Lenntech team for giving me this opportunity to pursue my graduation thesis in an interesting topic. Also, I would like to extend my gratitude to Dionysia and Armand for their kind help during my thesis.

I would like to thank my best mates Varun, Arya, Badri, Sushanth, Arvind, Shashish, Anoosh and the others for sharing this thrilling journey with me and helping me enjoy my time in Delft. Thanks to Rakesh, Varun and Sanjay for their ever-green support. I am eternally grateful to my parents and Anmol for believing in me, and for their constant support and encouragement.

Finally, I would like to thank my partner, my driving force and my source of strength, Samruddhi. Thank you for standing by my side during the toughest of times.

*Anurag Arun
Delft, December 2019*

Abstract

In this thesis, direct application of hollow fiber nanofiltration on surface water is suggested as an efficacious method for surface water treatment. This thesis was carried out as a collaborative effort between Lenntech B.V. and TU Delft. The current research aims to assess the performance of these membranes as a potential solution for surface water treatment and to gain a meaningful understanding of rejection performance and fouling tendencies of these modules through lab-scale experimentation of a low MWCO hollow fiber membrane. Direct application of nanofiltration on surface water was carried out on a lab-scale using the dNF-40 hollow fiber nanofiltration membrane supplied by NXFiltration B.V. Enschede. This membrane is fabricated using a technique called Layer-by-Layer (LbL) polyelectrolyte deposition which consists of an assembly of alternately deposited polycationic and polyanionic nanolayers on a polyethersulfone (PES) ultrafiltration support. The dNF-40 membrane is negatively charged at neutral pH. The main objective of the research was to determine the effectiveness of the dNF40 membrane for surface water treatment in terms of three key performance parameters viz. rejection, membrane fouling and concentration polarization. Membrane characterisation was carried out by measuring the pure water permeability, Molecular Weight Cut Off (MWCO) of the membrane and rejection of single salt solutions. The pure water permeability of a pristine membrane was 1.53×10^{-14} m. The MWCO was measured using PEG filtration method and was found to be 200 Da. The membrane performance is limited in terms of the flux due to concentration polarization. CP factor was measured experimentally and compared with Sherwood analytical model. Since the flow through the fibers in laminar, high cross-flow velocities are required to reduce CP are high (< 0.5 m/s) due to which hydraulic pressure losses along the feed channel are high. A pressure drop of 0.2 bar was measured for a pristine membrane at a cross-flow velocity of 0.5 m/s. Filtration experiments were carried out with two kinds of surface waters: Delft Schie water and Biesbosch reservoir water. The influence of flux and cross-flow velocity on the rejection of ions were investigated. The removal of Natural Organic Matter (NOM) in both surface waters was between 80 and 85%. The rejection of divalent cations viz. Ca^{2+} and Mg^{2+} was higher at low system recoveries (upto 30%) but a severe drop in rejection was observed at higher recoveries (80%). The final permeate collected at 80% recovery contained 37 mg/L of Ca^{2+} and less than 1 mg/L of NOM. 98% rejection of SO_4^{2-} was observed irrespective of the feed composition and operating conditions. The dNF-40 membrane exhibited high fouling-resistance during surface water filtration showing no mass transfer coefficient(MTC) decline during 6-hour experimental cycles with surface water. To test for fouling fractions of surface water, additional tests were carried out with model foulant solutions including sodium alginate, humic acid and bovine serum albumin with varying foulant concentrations and ionic strengths; of the three, alginate fouling was most severe in terms of flux decline. Irreversible fouling was observed during the alginate filtration tests. Fiber-blocking was also observed during alginate filtration due to aggregation of alginate and Ca^{2+} . Chemical cleaning with 200 ppm NaOCl solution at pH 12 completely restored the permeability. The results presented in this thesis demonstrate that the

dNF-40 hollow fiber membrane with the LbL structure can treat surface water without pre-treatment. These membranes are ideal for applications such as production of drinking water where partial removal of hardness and complete removal of organic matter is required.

Contents

Nomenclature	xi
Abbreviations	xiii
List of Figures	xv
List of Tables	xvii
1 Introduction	1
1.1 General Introduction	1
1.2 Scope and outline of thesis	2
2 Theoretical background	5
2.1 Structure and configuration of LbL hollow fiber membranes	5
2.2 Transport mechanisms through hollow fiber NF membranes	6
2.3 Rejection mechanisms in NF membranes	7
2.3.1 Steric Rejection	7
2.3.2 Donnan Effects	7
2.3.3 Dielectric exclusion	8
2.4 Membrane performance	8
2.4.1 Permeate flux	8
2.4.2 Hydraulic Pressure Loss	9
2.4.3 Recovery ratio	10
2.5 Membrane resistance	10
2.5.1 Fouling	10
2.5.2 Concentration polarization	11
2.6 Effect of operational parameters on membrane performance	13
2.6.1 Feed composition	13
2.6.2 Cross-flow velocity	13
2.6.3 pH and Temperature	14
3 Materials and Methods	15
3.1 Description of the experimental set-up	15
3.2 Membrane module	16
3.3 Experimental Procedure	17
3.4 Membrane characterization	18
3.4.1 Membrane water permeability	18
3.4.2 Molecular Weight Cut-Off	18
3.5 Concentration Polarization	20
3.6 Filtration Experiments	21
3.6.1 Single salt solutions	21
3.6.2 Surface water	21
3.6.3 Model foulant solutions	22

4	Results and Discussion	25
4.1	Permeability test	25
4.2	Molecular Weight Cut-off	25
4.3	Concentration polarization	27
4.4	Salt rejection	28
4.5	Surface water filtration	29
4.5.1	Delft Schie Water	29
4.5.2	Biesbosch reservoir water	31
4.6	Model foulant solutions	34
4.6.1	Sodium alginate	34
4.6.2	Humic Acid	37
4.6.3	Bovine serum albumin	40
5	Conclusions and Recommendations	41
5.1	Conclusions	41
5.2	Recommendations.	42
	Bibliography	45
A	MTC Measurement of Biesbosch water	53
B	Rejection of ions present in Biesbosch water	55
C	Concentration polarization during PEG experiment	57
D	Rejection of NOM in Schie Water	59

Nomenclature

Greek Symbols

β	Concentration polarization factor	[-]
δ	Concentration boundary layer thickness	[nm]
$\Delta\pi$	Osmotic pressure difference	[Pa]
ϵ_o	Permittivity of free space	$[8.85 \times 10^{-12} \text{ F/m}]$
ϵ_r	Relative permittivity of background solution	[80]
γ	Recovery ratio	[-]
κ^{-1}	Debye length	[Å°]
λ	Darcy friction factor	[-]
μ	Dynamic viscosity	[Pa.s]
ν	Kinematic viscosity	$[\text{m}^2/\text{s}]$
π_f, π_p, π_m	Osmotic pressure of feed, permeate and membrane wall	[Pa]
ψ	electric potential	[mV]
ρ	Density	$[\text{kg}/\text{m}^3]$
$\sigma(MW)$	Reflection coefficient	[-]
τ	Tortuosity	[-]

Latin Symbols

ΔP	Transmembrane pressure	[bar]
A_{cs}	Cross-sectional area of fiber	$[\text{m}^2]$
D	Diffusion coefficient	$[\text{m}^2/\text{s}]$
d_H	Fiber hydraulic diameter	[mm]
d_p	Stokes diameter	[nm]
d_{pore}	Pore diameter	[nm]
dc_i/dx	Concentration gradient	[M/m]
dP_{hydr}	Hydraulic pressure loss	[bar]
e	Elementary charge	$[1.6 \times 10^{-19} \text{ C}]$
F	Faraday constant	[96,485.3329 sA/mol]

J	Permeate flux	[Lm ⁻² h ⁻¹]
k	Mass transfer coefficient	[m]
K_B	Boltzmann constant	[1.38×10 ⁻²³ m ² kg s ⁻² K ⁻¹]
K_w	Pure water permeability	[m]
$K_{c,i}$	Convective hinderance	[-]
$K_{d,i}$	Diffusive hinderance	[-]
L	Channel length	[mm]
l	Pore thickness	[nm]
m	Molality	[mol/kg]
MW	Molecular Weight	[Da]
N	Number of fibers per module	[-]
N_A	Avogadro Number	[6.023×10 ²³]
p	Porosity	[-]
Q_f	Feed flow rate	[L/h]
R	Universal gas constant	[8.3142 J K ⁻¹ mol ⁻¹]
$R(\%)$	Solute rejection	[%]
R_A	Resistance due to adsorption	[m ⁻¹]
R_C	Resistance due to cake formation	[m ⁻¹]
R_G	Resistance due to gel formation	[m ⁻¹]
R_m	Clean membrane resistance	[m ⁻¹]
R_P	Resistance due to pore blocking	[m ⁻¹]
r_p	Stokes radius	[nm]
$R_{\Delta\pi}$	Resistance due to osmotic pressure	[m ⁻¹]
Re	Reynolds number	[-]
s_{MW}	Standard deviation of molecular weight distribution	[Da]
Sc	Schmidt number	[-]
Sh	Sherwood number	[-]
T	Absolute temperature	[K]
V_F	Initial feed volume	[L]
V_f	Cross-flow velocity	[m/s]

V_p	Volume of permeate produced	[L]
z	Membrane thickness	[nm]
z_i	Charge number of solute 'i'	[-]

Abbreviations

BSA	Bovine Serum Albumin
CEFF	Chemically Enhanced Forward Flush
CF	Concentration Factor
CP	Concentration Polarization
dNF	Direct Nanofiltration
EC	Electrical Conductivity
EPS	Extracellular Polymeric Substances
FF	Forward Flush
HPLC	High Performance Liquid Chromatography
IC	Ion Chromatography
LbL	Layer-by-Layer
MW	Molecular Weight Cut-off
MTC	Mass Transfer Coefficient
NDP	Net Differential Pressure
NOM	Natural Organic Matter
PAA	Polyacrylic acid
PAAM	Poly(allylamine)
PDADMAC	Polydiallyldimethylammonium chloride
PE	Polyelectrolyte
PEG	Polyethylene Glycol
PEI	Polyethylenimine
PES	Polyethersulfone
PSS	Polystyrene sulfonate
PVC	Polyvinyl Chloride
RIS	Resistance in Series
RO	Reverse Osmosis
RR	Recovery Ratio
TCF	Temperature Correction Factor
TFC	Thin Film Composite
TMP	Transmembrane Pressure
TOC	Total Organic Carbon
SA	Sodium Alginate
SEC	Size Exclusive Chromatography
SUR	Specific Ultrafiltration Resistance
VFD	Variable Frequency Drive

List of Figures

2.1	Flow of liquid through a hollow fiber membrane [14]	5
2.2	Layer-by-Layer assembled NF membrane. Adopted from [22]	6
2.3	Concept of concentration polarization [7]	12
3.1	dNF experimental set-up	15
3.2	Calibration curve from PEG retention test	19
4.1	Permeate flux at different TMPs	25
4.2	MWCO measurement of the dNF-40 membrane. A) 20 L m ⁻² h ⁻¹ B) 30 L m ⁻² h ⁻¹	26
4.3	Concentration polarization factor as a function of cross-flow velocity	28
4.4	Salt rejection by dNF-40 membrane (20 Lm ⁻² h ⁻¹)	29
4.5	Influence of cross-flow velocity on rejection of ions in Delft Schie	30
4.6	Influence of permeate flux on rejection of ions in Delft Schie	30
4.7	Mass transfer coefficient measurement during Schie water filtration: V _f = 0.5 m/s, J= 20 L m ⁻² h ⁻¹	31
4.8	Concentration of Ca ²⁺ in the permeate with at different recoveries. P _{mix} represents the mixed permeate	32
4.9	Ca ²⁺ rejection with increasing recovery with respect to concentration in the feed tank	33
4.10	NOM rejection with increasing recovery with respect to concentration in the feed tank	33
4.11	Concentration of ions and NOM in the feed and mixed permeate	34
4.12	MTC measurement during sodium alginate filtration. SA=100 mg/L, Ca ²⁺ =3mM	34
4.13	MTC measurement during sodium alginate filtration. SA=200 mg/L, Ca ²⁺ =3mM	35
4.14	Fiber(capillary) blocking mechanism[85]	36
4.15	MTC measurement during sodium alginate filtration. SA=100 mg/L, Ca ²⁺ =4 mM	36
4.16	MTC measurement during sodium alginate filtration. SA=100 mg/L, Ca ²⁺ =3 mM, pH=4.0	37
4.17	MTC measurement during humic acid filtration. HA=10 mg/L, Ca ²⁺ =1 mM	38
4.18	MTC measurement during humic acid filtration. HA=20 mg/L, Ca ²⁺ =3 mM	38
4.19	MTC measurement during humic acid filtration. HA=10 mg/L, Ca ²⁺ =3 mM	39
4.20	LC-OCD chromatogram of Delft Schie [88]	39
4.21	MTC measurement during humic acid filtration. BSA=20 mg/L, Ca ²⁺ =3 mM	40
A.1	Mass transfer coefficient measurement during Biesbosch water filtration: CFV= 0.5 m/s	53
B.1	Rejection of ions in Biesbosch water with respect to A) initial feed concentration and B) actual concentration of ion in the feed tank	55
C.1	Concentration polarization factors of different PEG MW fractions	57

D.1	Influence of cross-flow velocity on rejection of NOM in Schie Water.	59
D.2	Influence of flux on rejection of NOM in Schie Water.	59

List of Tables

1.1	Various module geometries of NF membranes [2, 6].	2
2.1	Various relations for mass transfer coefficients	13
3.1	Parts of the experimental set-up.	16
3.2	Membrane module specifications	17
3.3	Operating conditions	18
3.4	Average surface water quality of the two surface water sources	21
3.5	Summary of test conditions and operating parameters used during surface water filtration	22
3.6	Feed composition for alginate tests	23
3.7	Feed composition for humic acid and BSA tests	24
4.1	Calculated (Sherwood) and measured values of CP factor	27
4.2	Salt rejections of various NF membranes	28
C.1	Diffusion coefficients of PEG molecules	58

Introduction

1.1. General Introduction

Surface waters such as rivers, lakes and canals are usually highly contaminated by human wastes and industrial run-offs. They usually contain high concentrations of suspended solids, biological agents, inorganic and organic compounds. Natural organic matter (NOM) is the broad term used for a mixture of organic compounds found in water. The colour and odour of surface water is derived from different sources such as humic acids, peat material, different kinds of plankton, plant components, metal ions and also industrial wastes [1]. An increasing demand of high quality waters and stricter environmental rules require the need of advanced treatment techniques capable of producing high quality water at minimal costs and high efficiency.

Membrane filtration is a separation process in which the membrane acts as a selective barrier to restrict the passage of various contaminants [2]. It offers several advantages such as high quality of treated water (permeate), a smaller footprint, better hydrodynamic control and maintenance, fewer chemicals, and no production of sludge [3]. Pressure driven membrane filtration in water treatment can be broadly classified into two distinct groups based on the type of contaminant which is rejected by the membrane [4].

1. *Microfiltration and Ultrafiltration (MF/UF)* are used for the removal of particulate matter, viruses and bacteria.
2. *Nanofiltration and Reverse Osmosis (NF/RO)* are used for removal dissolved matter including organic molecules, ions and micropollutants such as pharmaceutically active compounds and pesticides.

Nanofiltration is a type of membrane process which offers a potentially cost-saving alternative to the conventional treatment process as well as reverse osmosis. It is a driven process with 75-99% rejection of multivalent ions, high rejection of organic micropollutants and complete removal of biological activity [5]. The performance of membranes for a given application largely depend on the module geometry. The classification of membrane modules based on their geometry is shown in table 1.1.

Spiral wound membranes have a high packing density but require extensive feed water treatment. The necessity of feed and permeate spacers in spiral wound modules increases the fouling tendency of these membranes [7]. Tubular membranes

Table 1.1: Various module geometries of NF membranes [2, 6]

	Spiral Wound	Tubular	Capillary/Hollow-Fiber
Packing density(m^2/m^3)	500-1000	100-500	1000-5000
Energy Usage	Low	Moderate	Moderate
Fouling tendency	High	Low	Low
Cleaning	Difficult	Backflush possible	Easy to clean

are easier to clean but generally have low packing densities and are expensive. Hollow fiber NF membranes have shown great promise for surface water treatment owing to their fouling-resistant nature and ease of cleaning [8]. Additionally, hollow fiber membranes are amenable to surface modification techniques which have been known to further improve the rejection and fouling characteristics of the membrane [9]. Layer-by-layer (LbL) polyelectrolyte deposition is an example of a surface modification, which consists of an assembly of alternately deposited polycationic and polyanionic nanolayers on an ultrafiltration support. Because of their channel geometry and ease of cleaning, hollow fiber NF membranes require minimal pre-treatment of feed water. Thus, it eliminates the need of several steps used in conventional surface water treatment processes including coagulation, flocculation and rapid sand filtration. Depending on the application of the produced water, advanced treatment such as granular activated carbon (GAC) adsorption and reverse osmosis (RO) might still be required. These steps can be replaced by a single nanofiltration step only preceded by a cartridge filter. This potentially results in a significantly lower footprint making it ideal for decentralised treatment schemes. This is known as direct nanofiltration (dNF).

In existing literature, the terms "capillary" and "hollow fiber" have been used interchangeably to describe ultrafiltration and nanofiltration membranes with several long filaments with small diameter (< 1 mm) packed in a single module [8, 10]. In contrast, the term "hollow fiber" has also been used to describe reverse osmosis membranes with extremely small fiber diameter ($1 \mu\text{m}$) [11]. However, in this thesis, the membranes with fiber diameter between 0.5 μm and 1 mm have been described as "hollow fiber membranes".

1.2. Scope and outline of thesis

Some pilot-scale studies have been conducted in the past to assess the rejection of ions by testing hollow fiber membranes with high MWCO (1000 Da) on real surface water [8, 12]. However, almost no studies have focused on low MWCO (< 400 Da) membranes fabricated using Layer-by-Layer (LbL) technique. Additionally, the fouling and rejection mechanisms have not been well-understood. The rejection of ions largely depends on the chemistry of the feed water and hydraulic parameters such as flux, recovery and cross flow velocity. The influence of these parameters on the overall performance has not been extensively studied owing to the limited laboratory-scale research on hollow fiber NF membranes.

Further progress on the implementation of hollow fiber membranes has been hampered due to the inadequate information about the performance of these membranes for specific applications such as surface water treatment. The current research aims to assess the performance of hollow fiber nanofiltration membranes as a potential solution for direct treatment surface water treatment and to gain a meaningful understanding of rejection mechanisms and fouling tendencies through lab-scale experimentation of a low MWCO hollow fiber membrane, dNF-40, supplied by NX-Filtration B.V., Enschede. The following two research questions were put forth to address the problem:

1. How is the performance of the dNF-40 membrane for the direct treatment of surface water in terms of the two performance indicators viz. rejection and fouling?
2. How can the development on the concentration polarization in the membrane be quantified?

The following sub-questions were formulated in order to answer the research questions:

- (i) What effect does the Layer-by-Layer structure have on rejection performance of the membrane?
- (ii) What is the dominant rejection mechanism of the membrane?
- (iii) What is the effect of operational flux, cross-flow velocity and recovery on the permeate quality?
- (iv) What is the flux decline during the filtration of surface water?
- (v) What fraction of NOM (polysaccharide, humics or proteins) has the highest fouling effect on the membrane and what is the dominant fouling mechanisms?
- (vi) What factors influence the occurrence of concentration polarization in the dNF-40 membrane?

Sub-questions (i), (ii) and (iii) provides an insight into the rejection performance of the membrane and the various parameters which influence the rejection of solutes. Sub-questions (iv) and (v) attempts to provide an answer to whether or not the membrane is fouling-resistant and the various parameters which influence the fouling rate. Sub-question (vi) answers the research question about concentration polarization in the dNF-40 membrane. This thesis is divided into five chapters:

Chapter 2 entails the literature review and detailed theory behind the working of hollow-fiber NF membranes. Initially, a description of the fabrication methods and the working of LbL configuration is provided. A detailed explanation of nanofiltration theory and principles including rejection theories, transport mechanisms in hollow fiber membranes, resistance mechanisms such as fouling and concentration polarization is presented.

Chapter 3 includes the details of materials and methods, a description of the experimental set-up and experimental procedures

Chapter 4 includes the results obtained from the experiments and a discussion of results is presented in order to answer the aforementioned research questions

Chapter 5 includes all the conclusions drawn from the results of the experiments. Finally, the recommendations from the author for future work in the field of hollow fiber NF membranes are discussed.

Theoretical background

2.1. Structure and configuration of LbL hollow fiber membranes

Hollow fiber membranes utilize several long, porous filaments with very narrow diameter. The fibers are packed in PVC shell. These fibers can be utilized to treat the feed water in either the inside-out or the outside-in configuration. In the inside-out configuration, the active membrane surface lies on the inner (lumen) side of the fiber. The feed flows on the inner surface in cross-flow mode and the permeate is collected on the shell-side. This kind of flow configuration is ideal for low fouling feed waters such as surface water since the feed channel is narrow causing a higher fouling load [13]. For outside-in filtration, the active surface lies on the outside of the fibers. Outside-in filtration is a better option for highly fouling feed such as sewage and/or municipal wastewater. Most commercial NF membranes are produced as

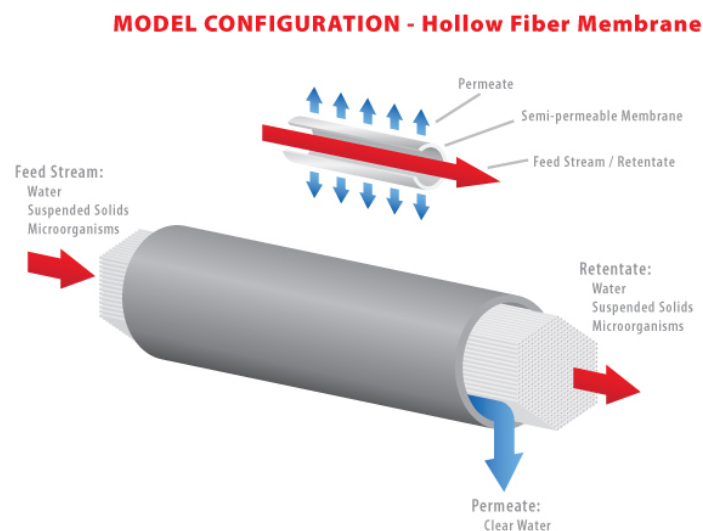


Figure 2.1: Flow of liquid through a hollow fiber membrane [14]

Thin Film Composite(TFC) flat sheet membranes which are fabricated using interfacial polymerization. Other methods of fabrication include grafting polymerization and nano-embedment have also been implemented [15, 16]. Single-layer hollow fiber ultrafiltration membranes have been frequently used for (waste)water treatment application since the early 1990s [3]. Recently, a class of multi-layer HF nanofiltration

membranes have been developed by Layer-by-layer (LbL) polyelectrolyte deposition method with chemical crosslinking [17]. The LbL assembly consists alternately deposited polycationic and polyanionic layers. Polyelectrolytes (PE) are long-chain molecules with a molecular weight of several kDa that have a functional group within the repeating unit that dissociates in water to a polycation or polyanion i.e. a positively or negatively charged PE. They can be grouped as strong and weak PE: Strong PEs dissociate independently of pH, whereas the degree of dissociation is a function of pH for weak PE [18]. The surface charge can be effectively regulated by changing the terminal polyelectrolyte layer [19].

Some commercially available polyelectrolytes include poly(acrylic acid) (PAA), poly(vinyl sulfate), poly(styrene sulfonate) (PSS), poly(ethylenimine) (PEI), poly(allylamine) (PAAm), and poly(diallyldimethylammonium chloride) (PDADMAC)[20]. An additional method to increase the tightness and selectivity of the membranes was suggested by Wang et.al in which the LbL polyelectrolyte layer was cross-linked with glutaraldehyde [21]. Polyethersulfone (PES) is one of the most important polymeric materials

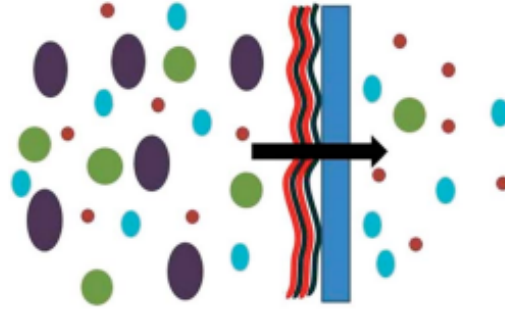


Figure 2.2: Layer-by-Layer assembled NF membrane. Adopted from [22]

which is used as an UF support. The sulfonyl group provides stiffness with a high glass transition temperature and along with the ring structures, makes the membrane chemically resistance. The ether linkages provide a degree of flexibility making it easy to process [23]. To reduce the hydraulic load on PES fibers, PES is often used as a material for inside-out filtration. These membranes have the advantage of working at extremely low pressures (2-5 bar) and yet provide efficient separation [17].

2.2. Transport mechanisms through hollow fiber NF membranes

The extended Nernst Planck Model proposed by Schloegl (1996) and Dresner (1972) can be used to describe ion transport through membranes [24, 25]. This differs from the commonly used Spiegler-Kedem model in which membrane is not treated as a 'black box' and hence attempts to explain the mechanism of solute transport across the membrane [26]. The extended Nernst-Planck equation describes the flux of a solute through the membrane active layer and can be given by equation 2.1 and 2.2.

$$j_i = -D_{i,p} \cdot \frac{dc_i}{dx} + K_{i,c} c_i J_v - \frac{z_i c_i D_{i,p} F}{RT} \cdot \frac{d\psi}{dx} \quad (2.1)$$

$$D_{i,p} = K_{i,d} D_{i,\infty} \quad (2.2)$$

where j_i flux of solute i , $K_{i,c}$ and $K_{i,d}$ are the convective and diffusive hindrance parameters respectively which depend on the pore size and solute Stokes radius, ψ is the electric potential, z_i is the ion valency, F is the Faraday constant, T is temperature and R is the universal gas constant. The first and second terms in equation 2.1 describe the diffusive and convective transport of material across the membrane while the third term describes the electromigrative transport. The negative sign preceding the diffusive and electromigration terms is because they occur down the concentration or electric gradient. However, convection occurs due to membrane porosity [17, 27].

2.3. Rejection mechanisms in NF membranes

A unique feature of nanofiltration membranes is that most of them possess surface charges in aqueous media. This means that solutes in the feed solution are rejected as a result of sieving effects as well as charge effects. This means that ions which have sizes much lesser than the pore size may also be rejected by the NF membranes. Rejection mechanisms occurring in nanofiltration membranes can be highly complex [28].

2.3.1. Steric Rejection

Steric rejection is based on pore size. Uncharged solutes are rejected by steric effects. Solutes smaller than the pore size pass through the membrane. The pore sizes of NF membranes are so small that it becomes difficult to measure it through conventional methods. Hence, a surrogate parameter called Molecular Weight Cut-Off (MWCO) is used. It is the size of the solute which is rejected with 90% efficiency by the membrane [29]. A standard method for measuring MWCO is by conducting filtration experiments using uncharged solute in the feed solution and measuring the rejection [30].

2.3.2. Donnan Effects

Donnan effects are significant for charged solutes and membranes with surface charge. The surface charge on the membrane is a result of dissociated functional groups like sulfonic or carboxylic groups. When placed in a salt solution containing charged ions, a Donnan equilibrium is set-up at the membrane-solution interfaces. This results in unequal charge distribution. The concentration of co-ions is lower on the membrane than in the solution but the concentration of counterions is higher [31, 32]. This difference in concentration of co and counterions sets up a potential difference at the interface. This potential difference, known as Donnan potential, prevents transport of ions between the membrane and solution. This effect thus increases the rejection of these ions. Due to the requirement of electroneutrality, the counter-ions are also rejected.

The distribution of ions in the solution leads to the formation of a double layer consisting of a charged surface and an adjacent layer of counter-ions in the solution [33]. In the Stern layer, the electric potential decreases linearly from the membrane surface potential. In the diffuse layer, the potential decays exponentially since the counter-ion concentration balances out the co-ion concentrations as the distance from the surface increases [34, 35]. The thickness of the electric double layer is characterized by the Debye length (κ^{-1}) and is given by equation 2.3 [36].

$$\kappa^{-1} = \left(\frac{\epsilon_0 \cdot \epsilon_r \cdot k_B \cdot T}{2000 \cdot N_A \cdot e^2 \cdot I} \right)^{\frac{1}{2}} \quad (2.3)$$

where ϵ_0 and ϵ_r are the permittivity of free space and the relative permittivity of the background solution respectively, K_B is the Boltzmann constant, T is the absolute temperature, N_A is the Avogadro's number, e is the elementary charge and I is the ionic strength given by:

$$I = \frac{1}{2} \sum m_i \cdot z_i^2 \quad (2.4)$$

For a given background solution and operating conditions, the Debye length is solely dependent on the ionic strength of the feed solution. At high ionic strength, the screening length is close to zero.

2.3.3. Dielectric exclusion

Dielectric exclusion is caused due to interactions of ions and the polarization charges at the surface of the membrane. The strength of the interactions is proportional to the square of the charge [37]. Different explanations for dielectric exclusion exist in literature. Bowen and Welfoot suggested that dielectric exclusion is caused by the solvation energy barrier between solvents with different dielectric constants [38]. The structure of the nano pore causes the realignment of the solvent molecules in different layers causing a change in its dielectric constant. Water molecules tend to polarize inside the pores due to high dipole moment (1.84 D or 6.33×10^{-30} C.m). The polarization decreases the dielectric constant inside the pore which prevents charged solutes in the bulk to enter the membrane pore. Additionally, ions undergo hydration in aqueous solution. Permeability of ions through NF membranes shows strong dependence on hydrated radii [39]. The complete mechanisms behind dielectric exclusion is not very well understood.

Regardless of these electric effects, the requirement for electroneutrality of permeate and feed, given in equations 2.5 and 2.6, has a significant impact on the rejection characteristics of the nanofiltration membrane. For instance, the rejection of co-ions due to Donnan effect will force the rejection of counter-ions. However, the presence the counter-ions on the permeate side will result in the passage of the co-ions as well [31].

$$\sum z_i \cdot c_{i,w} = 0 \quad (2.5)$$

$$\sum z_i \cdot c_{i,p} = 0 \quad (2.6)$$

2.4. Membrane performance

2.4.1. Permeate flux

The membrane performance can be expressed in terms of the permeate flux parameter. This parameter is given by the following general equation and is valid for all membrane processes [40]:

$$J = \frac{1}{\mu} \cdot \frac{\text{Driving force}}{\text{Resistance}} \quad (2.7)$$

where J is the liquid permeate flux and μ is the dynamic viscosity of the liquid. For nanofiltration membranes used in water treatment applications, the equation can be modified into equation 2.8.

$$J_w = \frac{1}{\mu_w} \cdot \frac{\Delta P}{R_m} \quad (2.8)$$

The term $1/R_m$ is defined as the Mass Transfer Coefficient (MTC) of the membrane and is denoted by K . For a clean membrane and pure water, this quantity can be established by measuring the flux of pure water as a function of the trans-membrane pressure. The slope of J_w against the TMP gives the pure water permeability of the membrane. Measurement of the water permeability of the membrane helps to determine if fouling has occurred in the membrane. Water permeability depends on the various factors such as pore size, thickness, porosity, tortuosity and surface properties of the membrane [30].

$$K_w = \frac{p d_{pore}^2}{8\tau l} \quad (2.9)$$

For a feed solution containing dissolved solutes, the driving force can be described as the difference between the TMP and the osmotic pressure gradient across the membrane. An increase in solute concentration in the feed, decreases the driving force and hence the permeate flux is lower than the flux of pure water

$$J = \frac{K_w}{\mu} \cdot (\Delta P - \Delta\pi) \quad (2.10)$$

2.4.2. Hydraulic Pressure Loss

Hydraulic losses occur during the flow of water from the feed side to concentrate side. The primary reason for hydraulic pressure losses is wall friction. Under steady state operating conditions, the flow in the fibers is expected to be in the laminar regime. Under laminar conditions, the flow is locally fully developed [41]. The pressure drop over the feed channel can be given by the Darcy-Weisbach model shown in equation 2.11 [42]. This equation is valid for $\frac{d_H}{L} \ll 1$ and $\frac{L}{v_f} \ll 1$.

$$\Delta P_{hydr} = \lambda \left(\frac{L}{d_H} \right) \cdot \left(\rho \frac{V_f^2}{2} \right) \quad (2.11)$$

Where λ is the Darcy friction factor, L is the length of the channel, d_i is inner diameter of the fiber and V_f^2 is the cross-flow velocity through the feed channel. For laminar flow through a hollow fiber structure, $\lambda = \frac{64}{Re}$ and $Re = \frac{d_H v_f \rho}{\mu}$. Pressure drop in the membrane is directly proportional to the length of the module. Pressure drop across

the membrane gives an indication of physical plugging or scaling. Vrouwenhouder et.al also studied that increase in pressure drop in NF membranes due to biofilm formation [43]. Another reason for increased pressure drop could be blocking or plugging of individual fibers by aggregates or flocs. This is because the plugging of fibers causes the liquid to flow with higher velocity through the unblocked capillaries which increases the friction in the fibers. An excessive pressure drop can cause the membrane or materials of construction to operate under higher stress, thereby causing damage to the membrane components and eventually resulting in a complete failure of the membrane.

2.4.3. Recovery ratio

For a batch filtration process, recovery (γ) is defined as the ratio of the quantity of the permeate produced (V_p) to the quantity of the feed (V_f).

$$\gamma = \frac{V_p}{V_f} \quad (2.12)$$

As the recovery ratio increases, the concentration of the feed solution increases in terms of the retained solutes. A small increase in system recovery can have a significant impact on the overall level of salts in the concentrate stream. The concentration factor(CF) of the feed can be calculated using equation 2.13.

$$CF = \frac{1}{1 - \gamma} \quad (2.13)$$

This means that a recovery ratio of 75 percent would increase the salt concentration factor to 4 and a recovery of 80 percent would result in a concentration factor of 5. Increased recovery causes the residual feed osmotic pressure to increase. In some cases, even a very small percentage increase in system recovery will exceed the solubility limit of some salts and result in higher fouling rates. At higher recoveries, concentration polarization is higher which leads to deterioration of permeate quality. Recovery is an important performance parameter. While a higher system recovery is often desirable in order to minimize concentrate production, a compromise is necessary to ensure that an acceptable permeate quality is maintained during filtration [27].

2.5. Membrane resistance

2.5.1. Fouling

Fouling is a significant technical challenge for membrane process which is manifested by increase in TMP required to produce permeate at constant flux. Most membrane fouling during the treatment of natural waters is caused by Natural Organic Matter (NOM) [44]. Membrane fouling is influenced by several operational parameters as well as solution chemistry making it difficult to model or predict. Fouling can be classified as internal (pore) and external (surface) or on basis of reversibility as reversible and irreversible fouling. Fouling can occur via five mechanisms. The Resistance in Series Model given in equation 2.14 describes the flux of a fouled membrane [45].

$$J = \frac{\Delta P}{\mu(R_m + R_{\Delta\pi} + R_A + R_G + R_P + R_C)} \quad (2.14)$$

where R_m is the clean membrane resistance, $R_{\Delta\pi}$ is the resistance due to osmotic pressure of the feed solution, R_A is the resistance due to adsorption, R_G is the resistance due to gel formation, R_p is the resistance due pore fouling and R_C is the resistance due to cake formation. The type of fouling depends on type of solute, the size of the particles and the interaction between the membrane and solute. The main mechanisms of fouling are:

1. *Complete pore blocking*: Particles larger than the pore are blocked and get deposited on the pore resulting loss in membrane surface and therefore decrease in permeate flux.
2. *Internal pore plugging*: Some small particles can go through the pore opening and get adsorbed or deposited on the walls of the pore causing restriction to flow of permeate decrease in permeate flux.
3. *Intermediate pore blocking*: Particles may partially block the pore by depositing on an inactive surface near the pore. Two or more particles causing intermediate pore blocking can lead to complete blocking of the pore [46].
4. *Cake/Gel formation*: Layers of particles get deposited on the surface of the membrane to form a “cake” layer. The feed solution then passes through the cake layer and then through the pores onto the permeate side. The total resistance to the flow is then the sum of the resistance offered by the cake and resistance of the membrane which could already be fouled by one of the mechanisms mentioned above. It is assumed that cake filtration itself does not block the pores.
5. *Biofouling*: Biofouling is the formation of biofilms on the membrane surface. The bacteria in the feed water get attached to the membrane, multiply and produce a slimy gel-like material called extra-cellular polymeric substances(EPS) [47]

A strict division of different types of fouling is not possible because a wide range of foulants are normally present in surface water. A combination of foulants can lead to the occurrence of various fouling mechanisms simultaneously [48].

2.5.2. Concentration polarization

Concentration Polarization (CP) refers to the build-up of concentration gradients at the membrane surface. Unlike fouling, the solutes do not deposit on the membrane surface or inside the membrane pores, but builds up close to the membrane surface [49]. An equilibrium is set up between the convective transport of material towards the membrane, and the diffusive transport of the rejected solute away from the membrane surface. The concept of concentration polarization is shown in figure 2.3. If CP becomes extensive, the concentration of the solutes at the membrane surface may be higher than the solubility limit which could lead to fouling and scaling [50]. The accumulation of solutes at the membrane surface causes an increase in osmotic pressure. According to equation 2.10, when the osmotic pressure, $\Delta\pi$ increases, the net driving force for the filtration decreases which leads to flux decline. This causes the observed solute rejection to drop as a result of low solvent permeation [51, 52].

In order to reduce the negative impacts of concentration polarization, cross-flow filtration should be used rather than dead-end filtration. This is because the flow in the direction parallel to the membrane sweeps the solute off the surface and reduces

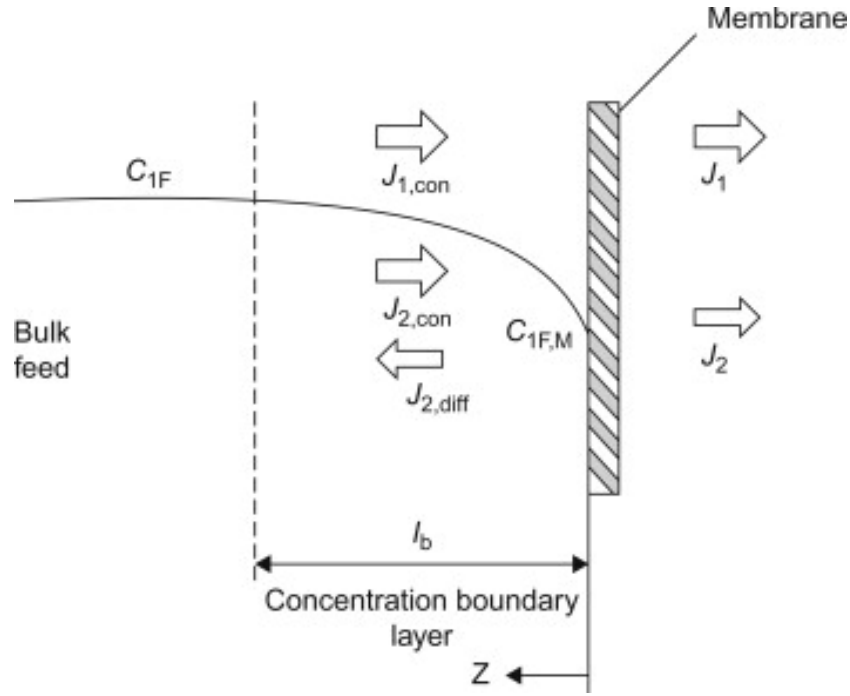


Figure 2.3: Concept of concentration polarization [7]

the accumulation. This is in contrast to dead-end filtration wherein the concentration boundary layer is infinitely large [53]. The thickness of the boundary layer is dependant on flow hydrodynamics and flow regime. At turbulent flow conditions, the effect of the concentration polarization is small. For laminar flow, the effect of the concentration polarization becomes considerable, resulting in a lower permeate flux [53]. Baker suggested that CP is better controlled in hollow fiber membranes working in inside-out fashion because dead-zones and stagnant areas are avoided in such a configuration [54].

A mass balance can be set-up at the membrane surface and can be given by equation 2.15.

$$J_i \cdot C_i = J_i C_{i,P} - D_{ji} \cdot \left(\frac{dC_i}{dz} \right) \quad (2.15)$$

Integrating equation 2.15 by taking the boundary conditions $z = 0$, $C_i = C_{i,M}$ and $z = \delta$, $C_i = C_{i,F}$ yields,

$$J_i = \frac{D_{ji}}{\delta} \ln \left(\frac{C_{i,M} - C_{i,P}}{C_{i,F} - C_{i,P}} \right) \quad (2.16)$$

where D_{ji} is the diffusivity constant of solute i in solvent j , δ is the boundary layer thickness, $C_{i,M}$, $C_{i,P}$ and $C_{i,F}$ are the concentration of species i on the membrane surface, in the permeate and in the bulk phase respectively. The term δ_{ji} is the mass transfer coefficient and is denoted by $k_{i,F}$. For a single species and water as solvent, equation 2.16 can be rewritten as:

$$J = k \cdot \ln \left(\frac{C_M}{C_F} \right) \quad (2.17)$$

The mass transfer coefficient, k , can be calculated using Sherwood correlation as

follows:

$$Sh = a \cdot Re^b \cdot Sc^c \cdot \left(\frac{d_H}{L}\right)^d = k \cdot \frac{d_H}{D} \quad (2.18)$$

where Sc is the Schmidt number given by $Sc = \nu/D$. The table 2.1 lists the common relations for mass transfer coefficients used in practice. For a hollow fiber system with laminar flow, the variables in equation can be described as $a = 1.62$, $b = 0.33$, $c = 0.33$ and $d = 0.33$ [7].

Table 2.1: Various relations for mass transfer coefficients

Equation	Flow regime	Reference
$Sh = 1.62 \cdot (Re \cdot Sc \cdot d_H/L)^{0.33}$	Laminar flow in a hollow fiber	[7]
$Sh = 1.85 \cdot (Re \cdot Sc \cdot d_H/L)^{0.33}$	Developing laminar flow in rectangular channel	[55]
$Sh = 1.5 \times 10^4 \cdot (Re^{0.47} \cdot Sc^{0.33} \cdot (K_w/d_H)^{0.35})$	Flow in circular channel ($2662 < Re < 21702$)	[56]
$Sh = 1.86 \cdot (Re \cdot Sc)^{0.33} \cdot (d_H/L)^{0.5}$	Fully developed laminar flow in hollow fiber	[57]
$Sh = 0.023 \cdot Re^{0.8} \cdot Sc^{0.33}$	Turbulent flow	[58]
$Sh = 0.023 \cdot Re^{0.875} \cdot Sc^{0.25}$	Turbulent flow in flat channel	[59]

2.6. Effect of operational parameters on membrane performance

2.6.1. Feed composition

Divalent ions are usually better rejected than monovalent ions. For negatively charged membranes, the cations in the feed solution migrate to the membrane surface due to the Donnan effect. Smaller ions such as sodium will pass through the membrane. In order to maintain electroneutrality, co-ions such as sulphate and chloride will also pass through the membrane. Chloride has higher permeability than sulphate due to its smaller hydrated radius and lower ionic charge [60]. Since chloride rejection is unaffected by increase in ionic strength, more sulphate ions need to be transported through the membranes to maintain electroneutrality. Hence rejection of polyvalent ions is higher at high ionic strengths [61]. In addition to the charge and size effects, the chemical interactions between various species in the feed could have a marked effect on the rejection characteristics of the membrane.

2.6.2. Cross-flow velocity

The cross-flow velocity determines the thickness of the concentration polarization layer. Higher cross-flow velocity decreases the thickness of the layer. For hollow fiber dNF membranes, the manufacturer recommends a cross-flow of $0.2\text{-}0.5 \text{ ms}^{-1}$. Based

on this cross-flow, the flow is expected to be laminar which suggests concentration polarization could play an important role in determining the efficiency in rejection of solutes.

2.6.3. pH and Temperature

pH influences the properties of the membrane and solutes. The surface charge of the membranes is directly related to the pH of the aqueous solution it is placed. For a negatively charged membrane, at high pH, the retention of ionic solutes generally increases due to strong dissociation functional groups [62]. This increases the Donnan potential between the membrane and the solution and increases the retention. Increasing the pH might also cause repulsion between polymer chains making the membrane looser. When the ionic strength, the zeta potential becomes zero and the pH does not affect the zeta potential significantly [30]. The dNF40 PES membranes are expected to be negatively charged at neutral and alkaline pH. The feed temperature affects the structural properties of the membrane such as pore size and membrane thickness. In addition, it affects the properties of the feed such as viscosity and diffusivity. The water flux is higher at higher temperatures due to increase in pore radius [63].

Materials and Methods

3.1. Description of the experimental set-up

The experimental set-up, shown in figure 3.1 and summary of parts is shown in table 3.1 was a cross-flow separation unit consisting of a feed tank which contains the feed water. The temperature in the feed tank was controlled using a spiral water cooler. By adjusting the flow of tap water through the cooler, the temperature of the feed tank can be maintained effectively with an accuracy of $\pm 0.5^\circ\text{C}$. A rotary vane pump draws the solution from the feed tank at high pressure. The pressure indicators displayed the pressure on the feed, concentrate and permeate. Before the membrane module, a two cartridge filters of 125 micron were placed in parallel to filter out particles which could block the capillaries.

The flow through the filters was switched by closing or opening a gate valve. Filter 4 was used during cleaning procedures and filter 5 was used during the filtration experiments. The feed flow rate was measured using a rotameter with measuring range 60–600 l/h. The cross-flow velocity can be calculated from the feed flow using the equation 3.1.

$$V_f = \frac{Q_f}{N \cdot A_{CS}} \quad (3.1)$$

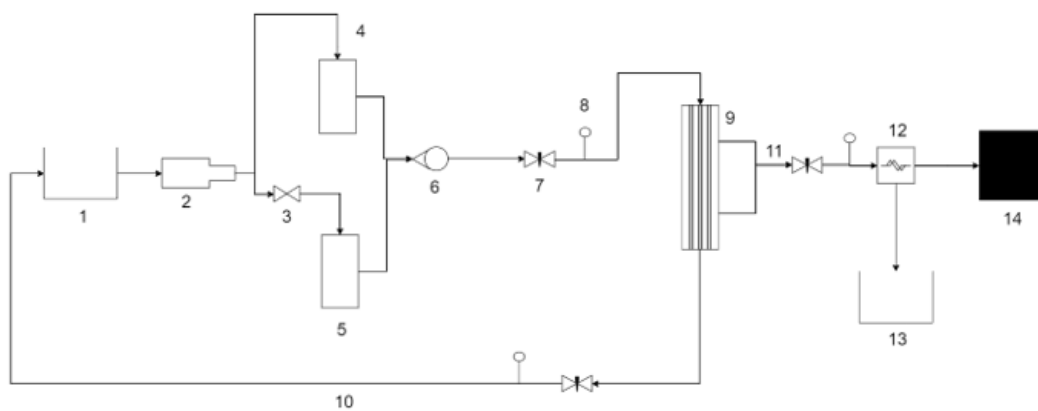


Figure 3.1: dNF experimental set-up

Table 3.1: Parts of the experimental set-up

Number	Part name	Additional comments
1	Feed Tank	10L, 20 L and 50 L
2	Pump	Rotary Vane (Fluid-o-Tech)
3	Check valve	Switch flow to filters
4	Cartridge filter	125 micron (for flushing)
5	Cartridge filter	125 micron (for experiments)
6	Rotameter	60-600 L/h
7	Needle valve	Flow adjustment on feed side (optional use)
8	Pressure indicator	0-10 bar (Wika Germany)
9	Hollow fiber NF module	dNF-40 (NXFiltration B.V.)
10	Concentrate	Recycled to feed tank
11	Permeate	Recycled or collected separately
12	Flow sensor	Flowbus(Bronkhorst Nederland)
13	Permeate tank	-
14	Monitor with data acquisition program	SUR:Measure

where Q_f is the feed flow rate, N is the number of hollow fibers in a module, A_{cs} is the cross sectional area of a single fiber given by $A_{cs} = \frac{\pi}{4} \cdot d_H^2$. The feed flow rate was adjusted using a variable frequency drive (VFD) connected to the pump. Increasing the frequency of drive results in higher suction which increases the cross-flow velocity. The feed water then passes through the hollow fibers and is filtered in inside-out fashion. The membrane splits the incoming feed water into a permeate stream and a concentrate stream. The concentrate was recycled to the feed tank. Needle valves were placed on the feed, concentrate and the permeate side. Needle valves were used for precise flow control. The needle valve on the feed side was not used since the flow was controlled by the VFD. The feed and concentrate pressure was changed by regulating the needle valve on the concentrate side. The feed, concentrate and permeate were read using pressure meters with measuring range 0-10 bar. The permeate was passed through a digital flow meter which continuously recorded the permeate flow, permeate flux and temperature. The data was logged and displayed on a monitor using a data acquisition software viz. SURP Measure.

3.2. Membrane module

The membrane module were supplied by NX Filtration B.V, Enschede. The membrane specifications are provided in table 3.2. The dNF membranes were manufactured using a “layer-by-layer” process where multiple nano-scale polycationic and polyanionic layers are deposited on PES support. The terminal polyelectrolytic layer

is negatively charged.

Table 3.2: Membrane module specifications

Parameter	Value
Name	dNF-40
Membrane material	Modified PES
Module length	300 mm
Membrane surface charge	Negative at pH 7
Fiber ID	0.7 mm
Operation	Inside-Out, Cross flow mode
Est. Bacteria rejection	>6 log
Maximum TMP	6 bar
Typical cross-flow	0.1-1.0 m/s
Operating pH range	1 to 14
Number of fibers in module	120

3.3. Experimental Procedure

Filtration experiments were carried out with different feed solutions. Before each experiment, demineralized water was circulated through the system for 20-30 minutes and a gravity drain was conducted to remove the water inside the system. After each experiment, a forward flush (FF) with demineralized water was conducted for around 10 minutes at 1.5 times the filtration velocity. Forward flush was carried out as a precautionary cleaning procedure and to avoid contamination of the feed for the next experiment. After the system shut-down, the membrane was submerged in demineralized water to prevent the fibers from drying out. In most of the experiments, the permeate was also recycled back to the feed tank to maintain constant feed concentration during the batch process. For the experiments to determine the effect of system recovery ratio on the performance of the membrane, the permeate was first collected in a separate container. Once the recovery ratio needed was achieved, the permeate was recycled to the feed tank and the filtration was carried out for 2 hours at the desired concentration factor.

Several samples of the feed and permeate were collected during the experiments. During each experimental run, the permeate samples were collected every 30 minutes and feed samples were collected every 1 hour. The samples also serve to minimize errors during analysis. The operating conditions used for the experiment are shown in table 3.3 (unless otherwise mentioned).

Table 3.3: Operating conditions

Parameter	Value	Unit
Cross-flow velocity	0.25, 0.5, 0.6, 0.75	<i>m/s</i>
Feed volume	10 L, 20 L	<i>L</i>
Permeate flux	20, 30	<i>L/(m²h)</i>
TMP	3.75	<i>bar</i>
Temperature	21	<i>°C</i>
Nominal Pressure drop	0.2	<i>bar</i>

3.4. Membrane characterization

3.4.1. Membrane water permeability

The water permeability of the membrane was calculated using equation 2.10 and trans-membrane pressure, ΔP was calculated using equation 3.2.

$$\Delta P = P_f + \frac{dP_{hydr}}{2} - P_p \quad (3.2)$$

where P_f and P_p are the pressures on the feed and permeate side respectively and ΔP_{hydr} is the hydraulic pressure loss across the feed channel. For pure water as feed, osmotic pressure is equal to zero. In order to determine the value of K_w , demineralized water was used as feed water and was filtered in cross-flow mode at varying TMPs at a constant temperature of 21°C. The constant cross flow of 0.6 m/s was maintained during the tests. The ratio of the permeate flux to the TMP gives the pure water permeability of the membrane. Due to the re-circulation of the concentrate to the feed, the temperature of the water in the feed tank increased slightly. The change in temperature affects the flow rate of the permeate. Hence, a temperature correction factor(TCF) was used to calculate the equivalent flux at 21°C [29].

$$J_{w,21^\circ C} = J_{w,T} \cdot e^{-0.0239 \cdot (T-21)} \quad (3.3)$$

where $J_{w,T}$ is the actual flux at temperature T and $J_{w,21^\circ C}$ is the flux corrected for 21°C.

3.4.2. Molecular Weight Cut-Off

The pore size of nanofiltration membranes usually ranges from 0.5 to 1 nm. The pore sizes and pore distributions are practically impossible to measure directly due to extremely small pore radii, Hence, the molecular weight cut off (MWCO) is often used as a surrogate parameter to estimate the rejection capacity of the membrane. MWCO is achieved at 90% rejection of various types of solutes with different molecular weights [64]. Currently, there is no standard procedure available for the determination of the MWCO of a membrane. However, a popular technique involves running multiple membrane filtration tests using a feed solution containing a homologous series of

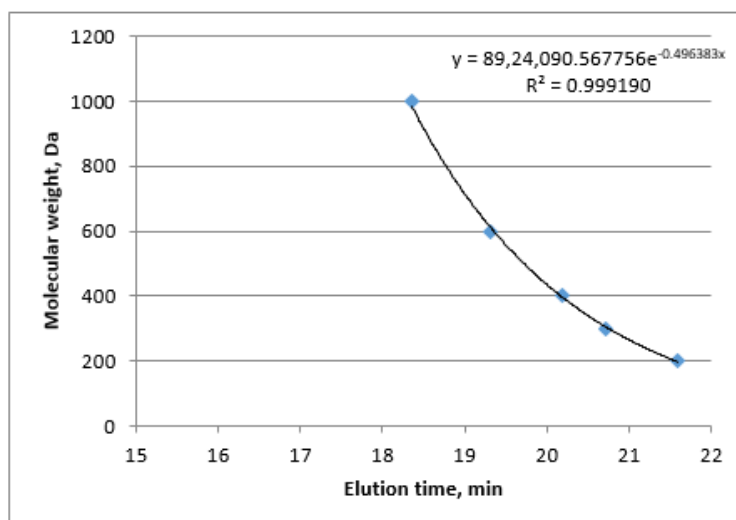


Figure 3.2: Calibration curve from PEG retention test

neutrally charged organic solutes [65]. MWCO determination is in itself a complicated procedure owing to the fact that its measurement is influenced by a variety of intrinsic as well as operational factors. Hence, it may vary with the method used to measure it. During this research, different molecular weights (100 Da — 1000 Da) polyethylene glycols were used as the tracer solute for MWCO determination. A mixture of PEGs (supplied by Sigma-Aldrich) with molecular weights of 200, 300, 400, 600 and 1000 Da in a concentration of 0.6 g/L each in deionized water was used as feed solution for filtration. To prepare the mixed solute feed solution, 6 g of each of the PEGs 200 to 1000 was weighed and mixed with 10 litres of ultrapure water and constantly stirred for 24 hours. The experiment was conducted at two different fluxes of 20 and 30 L m⁻²h⁻¹ to observe if the flux had any effect on the MWCO measurement of the membrane. Samples of the feed and permeate were collected every half hour and stored in the refrigerator at 5°C. The total time of each experiment was 2 hours.

Each sample was filtered using a 0.45µm filters and then analysed using high performance liquid chromatography system (HPLC, Shimadzu Japan) with a size exclusive chromatography column (SEC). The PEG molecules with different molecular weights show different elution times when passing through the columns. Each elution time corresponds to a specific molecular weight of PEG. The strength of the signal triggered by the PEG is proportional to the concentration of that PEG in the samples. Signal obtained from the HPLC measurements were subtracted from the baseline measurement to obtain the absolute intensities. Standard solutions of each PEG (200 - 1000 Da) with a concentration 0.6 g/L were prepared and analysed using HPLC to obtain the calibration curve. A calibration curve can be used to describe the relationship between the elution time and MW of PEG.

The PEG retention can be calculated using the equation:

$$R(\%) = \left(1 - \frac{C_{i,permeate}}{C_{i,feed}}\right) * 100 \quad (3.4)$$

where $C_{i,permeate}$ and $C_{i,feed}$ are concentrations of PEG of molecular weight 'i' in

the permeate and feed respectively. The rejection of PEGs was plotted against the molecular weights obtained from the calibration curve equation for the given time interval. This curve is called the experimental retention curve. The point at which 90% rejection is achieved on the retention curve is the value of the MWCO for the membrane. The rejection of PEGs was plotted against the molecular weights obtained from the calibration curve equation for the given time interval. This curve is called the experimental retention curve. The point at which 90% rejection is achieved on the retention curve is the value of the MWCO for the membrane. The retention curve can also be modelled by assuming a log normal distribution of pores given in equation 3.5 [29, 66].

$$\sigma(MW) = \int_0^{MW} \frac{1}{s_{MW}\sqrt{2\pi}} \cdot \frac{1}{MW} \cdot \exp\left(\frac{-\ln(MW) - \ln(MWCO) + 0.56s_{MW}}{2s_{MW}}\right) dMW \quad (3.5)$$

where $\sigma(MW)$ is the reflection coefficient of PEG of molecular weight MW and s_{MW} is the standard deviation of the molecular weight distribution. Shang et.al. suggested an empirical relation between the MWCO and the pore size of the membrane.

$$d_s = 0.065 \cdot (MW)^{0.437} \quad (3.6)$$

Further empirical relationships between membrane pore size and solute Stokes radius was suggested by Singh et.al. and Bowen and Mohammed[67, 68].

$$\log(r_s) = -1.3363 + 0.395\log(MW) \quad (3.7)$$

$$d_s = 0.1 \cdot (0.1673(MW))^{0.557} \quad (3.8)$$

3.5. Concentration Polarization

The Concentration Polarization Factor (CPF) can be defined as a ratio of salt concentration at the membrane surface (C_m) to bulk concentration (C_f). To measure concentration polarization in the membrane, 12 g/L $MgSO_4 \cdot 7H_2O$ was used as feed solution. The temperature of the feed tank was kept constant at 21°C. The osmotic pressure difference, $\Delta\pi$ is the difference between the osmotic pressure at the membrane wall (π_m) and the permeate (π_p) [53].

$$\Delta\pi = RT(C_m - C_p) = \pi_m - \pi_p \quad (3.9)$$

The concentrations of salt in the feed and permeate were measured in terms of the electrical conductivity of the solutions. Concentration and EC of $MgSO_4 \cdot 7H_2O$ follow almost a linear relationship [53]. The new permeate flux can be obtained by modifying Equation 2.10

$$J = \frac{K_w}{\mu} \cdot (\Delta P - \pi_m + \pi_p) \quad (3.10)$$

The concentration polarization factor, β was calculated using equation 3.11

$$\beta = \ln\left(\frac{\pi_m}{\pi_f}\right) \quad (3.11)$$

The concentration polarization factor of the membrane was measured at cross-flow velocities of 0.25 m/s and 0.5 m/s and at fluxes of 20 $Lm^{-2}h^{-1}$ and 30 $Lm^{-2}h^{-1}$. An

increase in permeate flux increases the rate at which the ions reach the membrane surface and increases CP [69]. An increase of cross flow increases turbulence and reduces the thickness of the concentration layer near the membrane surface.

3.6. Filtration Experiments

Membrane filtration experiments were carried out with single salt solutions, surface water from Delft Schie and the Biesbosch lake as well as individual model foulants viz. sodium alginate, humic acids and bovine serum albumin. The filtration tests aim to answer the aforementioned research questions. A description of the test conditions and the feed water is provided in the following section.

3.6.1. Single salt solutions

Filtration experiments with single salt solutions containing $MgCl_2$, $MgSO_4 \cdot 7H_2O$, Na_2SO_4 and $NaCl$ in order to determine the rejection characteristics and rejection mechanisms of the membrane. The experiment was conducted at two different fluxes. The concentration of the salt used was 0.05 M. The rejection was determined by measuring the EC of the feed and the permeate.

$$R(\%) = \left(1 - \frac{EC_{perm}}{EC_{feed}}\right) * 100 \quad (3.12)$$

3.6.2. Surface water

Two types of surface water were used for the experiments viz. Delft Schie Water and Biesbosch reservoir water. The Biesbosch water was supplied by Evides B.V. Filtration tests were conducted and samples of the feed and permeate were collected every half hour while the Schie water was collected from the pipeline at the Water Lab in TU Delft. The average quality of the two surface waters is shown in table 3.4. The Biesbosch reservoir water has much lower hardness and TOC content than the Delft Schie Water. The Delft Schie also has higher ionic strength. The pH of the two waters are almost the same.

Table 3.4: Average surface water quality of the two surface water sources

Parameter	Delft Schie Water	Biesbosch Water
pH	7.6	7.2
Conductivity ($\mu S/cm$)	704	415
Calcium ($mmol/L$)	1.8	1.1
Sodium ($mmol/L$)	1.5	1.5
TOC(mg/L)	10.5	4

The flux of the permeate was monitored using a data logger for the entire length of the experiments. The ionic composition of the feed and permeate water samples were determined using ion chromatography (Metrohm 883 system, Metrohm, Switzerland). Prior to these analyses the samples were filtered through 0.45 μm filters (Whatman,

Table 3.5: Summary of test conditions and operating parameters used during surface water filtration

Exp No.	Water Type	Flux (Lm ⁻² h ⁻¹)	CF	Cross-flow velocity (m/s)	Average temperature (°C)	pH
1	Delft Schie Water	20	1	0.6	21.3	7.6
2	Delft Schie Water	30	1	0.6	21.3	7.6
3	Delft Schie Water	20	1	0.75	21.3	7.5
4	Delft Schie Water	20	1	1.0	21.3	7.6
5	Biesbosch Water	20	1	0.6	21.3	7.2
6	Biesbosch Water	20	1.25	0.6	21.3	7.2
7	Biesbosch Water	20	2	0.6	21.3	7.2
8	Biesbosch Water	20	5	0.6	21.3	7.2

Germany). An anion column was used with 3.2 mM Na_2CO_3 and 1 mM $NaHCO_3$ as eluent for anions. For the cations, a cation column with 3 mM HNO_3 eluent was used. 150 mM H_3PO_4 was used as regenerent solution for the column. NOM concentration of the feed and permeate were determined in terms of the total organic carbon (TOC) using a TOC analyser (Shimadzu). It uses the combustion catalytic oxidation and NDIR Method. Table 3.5 summarizes the test conditions and operational parameters used in the experiments.

3.6.3. Model foulant solutions

In order to achieve a better understanding of the fouling phenomena, three types of model compounds (representing different fractions of NOM) were used in this study viz. Sodium Alginate (Sigma-Aldrich), Humic Acid (Vitens) and Bovine Serum Albumin (Sigma-Aldrich).

Sodium Alginate

Sodium alginate is produced from brown algae. It is a linear, hydrophilic polyuronic acid composed primarily of anhydro- β -D-mannuronic acid residues. Alginate has been used as model polysaccharide in several studies [70–72]. Alginate mimics the behaviour of extracellular polymeric substances which are commonly found in natural waters and are known to cause severe fouling in membrane. Based on the manufacturer, the molecular weight of the alginate ranges from 12 to 80 kDa. Sodium alginate is negatively charged at neutral pH.

Calcium ions are known to bind selectively to the gluconic acid residues in the alginate molecules leading to cross-linking of alginate molecules. This cross-linking promotes the formation of a gel-like aggregates. The presence of divalent ions alters the zeta potential of the alginate solution. In addition, presence of divalent cations such as calcium ions also cause bridging between the membrane surface and organic molecules which promotes fouling [6]. This can be explained by the DLVO theory. The divalent cations causes a charge screening effect between the negatively charged membrane and the negatively charged alginate molecules thus making it easier from the alginate to be deposited via the Ca^{2+} bridge. Additionally, the Ca^{2+} also bridges

the existing alginate fouling layer with the new fouling layer. Jamaal et.al reported that the measurement of the zeta potential of the 1 g/L alginate was reduced from -70.3 mV to -46 mV when Ca^{2+} concentration added increased from 0 to 222.5 mg/L [73].

Hence, the fouling effect of sodium alginate solution was tested at concentrations of 100 mg/L and 200 mg/L and Ca^{2+} concentrations of 3 mM and 5 mM. 5mM of sodium chloride was added to increase the ionic strength of the alginate solution. Sodium bicarbonate was also added as buffer to maintain the pH of the solution at 7 ± 0.2 . Although sodium ions do not have a chelating (bridging) effect on the NOM, it still influences fouling by suppressing the electrical double layer of the alginate molecules [74]. It is unlikely to observe such high concentrations of polysaccharide NOM fraction in natural waters but these concentrations were chosen to observe accelerated fouling in the membrane. Van de Ven et.al. used a concentration of 50 mg/l SA in their study to get sufficient fouling [75]. Another important factor that plays a role in the fouling of the membrane is the solution pH. At lower pH, the functional groups on the membrane become protonated which increases the zeta potential (zeta potential becomes less negative). The carboxylic groups of the NOM are protonated at low pH. The feed composition used for the alginate experiments are shown in table 3.6

Table 3.6: Feed composition for alginate tests

Name	Foulant concentration (mg/L)	pH	Ionic composition
Sodium Alginate 1	100	7.2	3mM $CaCl_2 \cdot 2H_2O$ + 5mM $NaCl$ + 2mM $NaHCO_3$
Sodium Alginate 2	200	7.2	3mM $CaCl_2 \cdot 2H_2O$ + 5mM $NaCl$ + 2mM $NaHCO_3$
Sodium Alginate 3	100	7.2	5mM $CaCl_2 \cdot 2H_2O$ + 5mM $NaCl$ + 2mM $NaHCO_3$
Sodium Alginate 4	100	4.0	3mM $CaCl_2 \cdot 2H_2O$ + 5mM $NaCl$

Humic acid

Humic acid (HA), comprising a group of heterogeneous recalcitrant polymeric organics, is abundant in natural waters [76]. In general, NOM components, such as humic substances, are negatively charged in the normal pH range due to the dissociation of carboxylic (and phenolic) functional groups [45]. Unlike alginate molecules, humic acids are highly hydrophobic [77]. A 100 g/L solution of Humic Acid which was extracted from a drinking water treatment plant supplied by Vitens was used as stock solution to prepare Humic Acid solutions of 10 mg/L. Ca^{2+} concentrations of 1mM and 3 mM were tested.

Table 3.7: Feed composition for humic acid and BSA tests

Name	Foulant concentration (mg/L)	pH	Ionic composition
Humic Acid 1	10	7.2	1mM $CaCl_2 \cdot 2H_2O$ + 5mM $NaCl$ + 1mM $NaHCO_3$
Humic Acid 2	10	7.2	3mM $CaCl_2 \cdot 2H_2O$ + 5mM $NaCl$ + 1mM $NaHCO_3$
Humic Acid 3	20	7.2	3mM $CaCl_2 \cdot 2H_2O$ + 5mM $NaCl$ + 1mM $NaHCO_3$
Bovine Serum Albumin	20	7.1	3mM $CaCl_2 \cdot 2H_2O$ + 5mM $NaCl$ + 1mM $NaHCO_3$

Bovine Serum Albumin

BSA consists of a single polypeptide chain, containing around 583 amino acid residues and no carbohydrates. The molecular weight of BSA is around 66 kDa. BSA is negatively charged at neutral pH. The iso-electric point of BSA is 4.7. BSA can cross-link with Ca^{2+} via its free thiol-groups [74, 78]. BSA has been used as a model compound to represent protein fouling in membranes, especially in wastewater (municipal wastewater and sewage) treatment[79]. 20 mg/L of BSA was used as feed solution along with 3mM Ca and 3 mM Na.

Results and Discussion

4.1. Permeability test

Figure 4.1 shows the result of the permeability test conducted on the pristine membrane at a temperature of 21°C. The pure water permeability of the membrane was found to be 1.6667×10^{-14} m which is equivalent to a MTC of $6 \text{ L m}^{-2} \text{ h}^{-1} \text{ bar}^{-1}$. Diamantidou measured the pure water permeabilities of spiral wound membranes with similar pore sizes and under similar test conditions [30]. A comparison of the results shows that pure water permeability of the dNF-40 membrane is 9% lower than that of the Synder NFW (242 Da) spiral wound membranes and 160% lower than the Dow NF270 membrane. The lower water permeability of the dNF-40 is due to the incorporation of the polyelectrolyte multilayers which causes a decrease in the pore size of the membrane and increases the tortuosity.

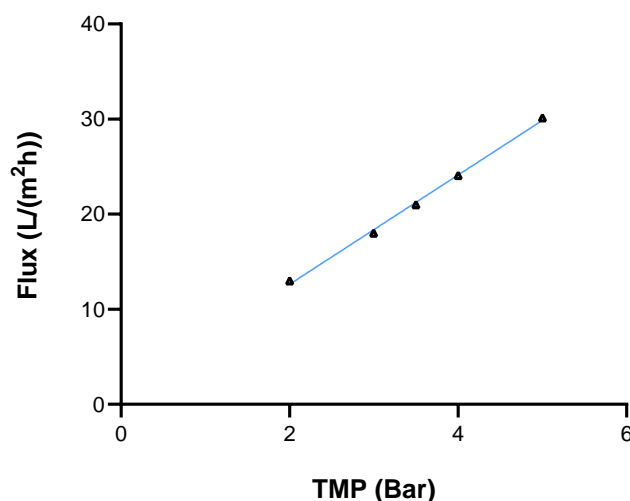


Figure 4.1: Permeate flux at different TMPs

4.2. Molecular Weight Cut-off

The measured MWCO of the dNF-40 membrane was found to be between 185 and 200 Da. The PEG Stokes radius calculated from equation 3.6 is 0.658 nm. Figure

4.2 shows the plot of MW of the PEG molecules to the rejection ratio of the membrane. This plot is known as the retention curve. The MWCO of the membrane is the point at which 90% rejection or rejection ratio of 0.9 is obtained in the rejection curve. This is shown by the red point in figure 4.2. Membrane MWCO modeling was also conducted by assuming log-normal distribution of the pores in the membrane as discussed. The real rejection of PEG molecules by the membrane reasonably fits the log normal distribution curve. The MWCO measurement of the membrane reduces slightly as the permeate flux increases. The MWCO measured at $20 \text{ L m}^{-2} \text{ h}^{-1}$ is 10% higher than the MWCO at $30 \text{ L m}^{-2} \text{ h}^{-1}$. Similar results were also obtained in a previous research conducted with spiral wound NF270 membranes [80].

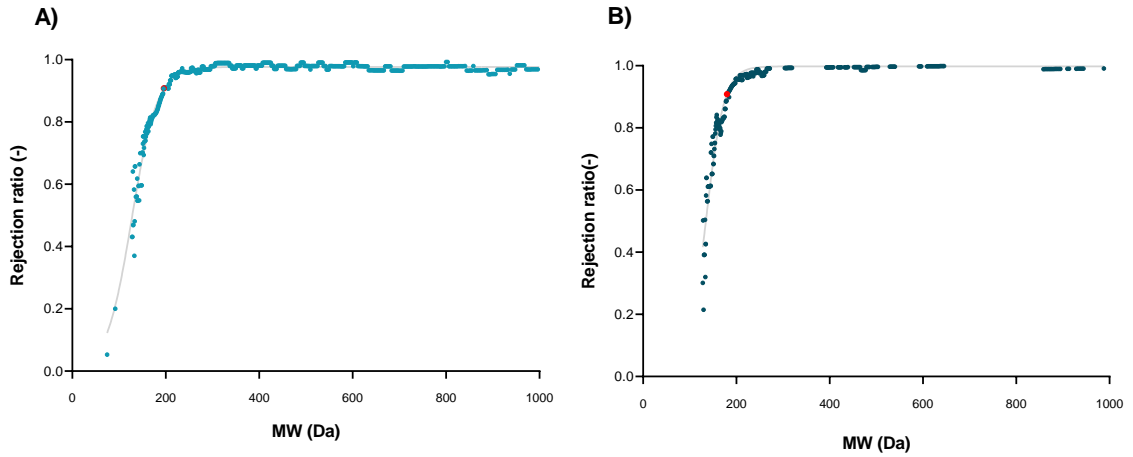


Figure 4.2: MWCO measurement of the dNF-40 membrane. A) $20 \text{ L m}^{-2} \text{ h}^{-1}$ B) $30 \text{ L m}^{-2} \text{ h}^{-1}$

For uncharged solutes such as PEG, solute transport can be best described by Spiegler-Kedem equation shown in equation 4.1 [81]. It mainly describes the transport as a sum of diffusive and convective flux. The convective flux, J_v is a pressure-dependent term while the diffusive term is independent of pressure. At higher TMP, the convection flux of the liquid is higher causing lower concentration of the solute in the permeate. Hence, the MWCO measurement of the membrane is slightly lower at higher flux.

$$J_s = -P_s \Delta x \frac{dc}{dx} + (1 - \sigma) J_v c \quad (4.1)$$

where P_s is the solute permeability and σ is the reflection coefficient of the solute. MWCO measurement is also influenced by operational parameters, feed composition and choice of tracers. This could explain the significant discrepancy between the measured values and the values provided by the manufacturer (400 Da). Using a mixture of PEGs as feed solution tends to underestimate the MWCO as larger molecules can block the permeation of smaller PEG molecules which is translated into a low MWCO [29].

Table 4.1: Calculated (Sherwood) and measured values of CP factor

Cross flow velocity		0.25 m/s		0.5 m/s	
TMP (bar)	Flux ($\text{Lm}^{-2}\text{h}^{-1}$)	Calculated	Measured	Calculated	Measured
3	6.46	1.13	1.21	1.11	1.16
5	15.11	1.36	1.62	1.31	1.48

4.3. Concentration polarization

Using the physical parameters of the membrane, the CP factor can be calculated using the Sherwood model with empirical constants. Table 4.1 shows the comparison between theoretical and calculated values of concentration polarization factor during the concentration polarization test. A comparison of CP factor calculated using Sherwood model and measured during experiments shows that the Sherwood model underestimates the concentration polarization effect in the dNF-40 membranes. At TMP of 3 bar, the Sherwood model shows a low deviation of 5%. At TMP of 5 bar, the error in the prediction increases to 19%. The difference between measured and calculated values is lower at high cross-flow velocities. A possible reason for this is the value of the diffusion coefficient chosen for calculation was higher than the real diffusion of the salt ions [82]. The performance of the membrane is limited in terms of the permeate flux. The risk of concentration polarization limits the permeate flux. For instance, at a flux of $30 \text{ L m}^{-2}\text{h}^{-1}$, the CPF is between 1.7 and 2.4 depending on the cross flow which means that the concentration of the solute at the membrane surface is almost twice as much as the feed concentration. If the salt concentration at the membrane surface exceeds saturation index, scaling will occur. To avoid CP at high fluxes, a very high cross flow velocity is required which entails significant energy costs and leads to increased hydraulic pressure losses across the membrane. Labban et.al. reported concentration polarization factors of 1.5 at 3 bar and upto 2.4 at 5 bar in the LbL1.5C hollow fiber nanofiltration membrane [17]. Figure 4.3 shows the estimated concentration polarization factors for the PEG filtration tests calculated using the Sherwood model for the dNF-40 membrane.

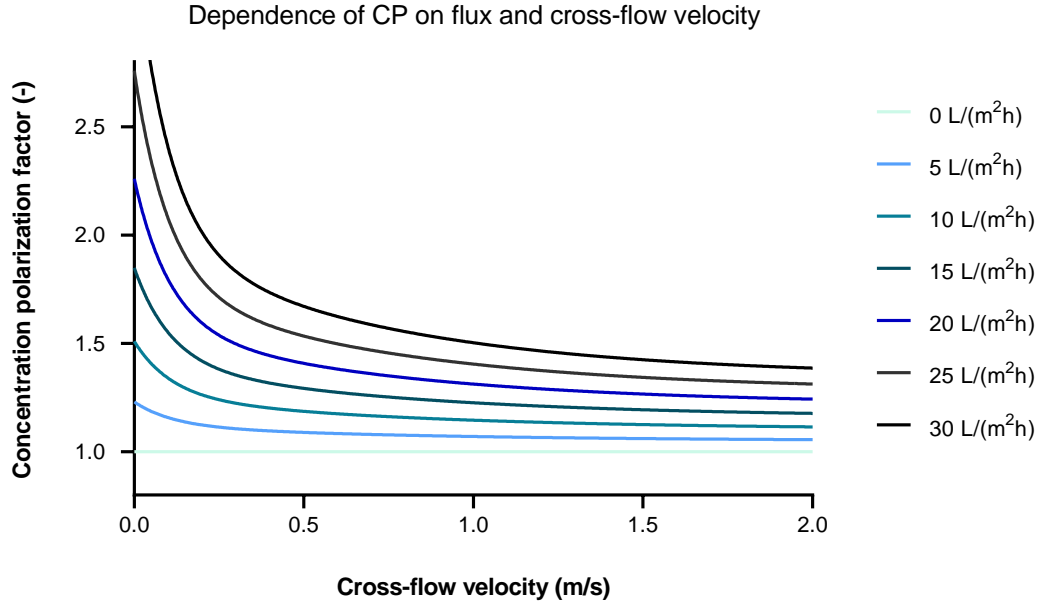


Figure 4.3: Concentration polarization factor as a function of cross-flow velocity

4.4. Salt rejection

The rejection plot for salt solutions containing single salts are shown in figure 4.4. The rejection of MgSO_4 is around 96% and Na_2SO_4 is 90%. The rejection of NaCl is 10% and MgCl_2 is 60%. The rejection of the membrane is thus primarily governed by the divalent anions such as sulphate due to the negatively charged terminal polyelectrolyte layer. This can be seen by comparing the rejection of Na_2SO_4 and NaCl . The rejection of SO_4^{2-} causes the Na^+ to also be rejected due to maintain electroneutrality of the solution. A comparison between single salt rejections by different nanofiltration membranes is shown in table 4.2. The MgCl_2 rejection by the dNF-40 is 30% higher than the NF270 membrane. This suggests that the positively charged multilayers increase the rejection of positively charged ions such as Mg^{2+} . In the study conducted by Liu et.al., the LBL2C membrane with a positively charged terminal layer at neutral pH, showed an MgCl_2 retention of 98% [21]. Thus, the layer-by-layer structure provides selective rejection of charged solutes which is one of the major advantages of these membranes.

Table 4.2: Salt rejections of various NF membranes

Membrane	MgSO_4 (%)	Na_2SO_4 (%)	NaCl (%)	MgCl_2 (%)	Reference
dNF-40	96.2	90	9.8	59.4	current study
LBL2C	93.0	15.0	58.6	98.1	[21]
NF-270	96.3	98.1	37.1	42.9	[21]

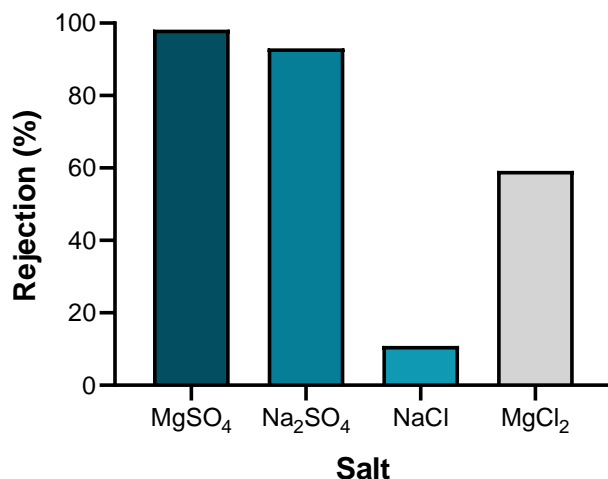


Figure 4.4: Salt rejection by dNF-40 membrane ($20 \text{ L m}^{-2} \text{ h}^{-1}$)

4.5. Surface water filtration

The aim of the section was to assess the performance of this membrane in treating two kinds of surface waters in The Netherlands. The performance of the membrane can be judged on the basis of two parameters viz. rejection and fouling.

4.5.1. Delft Schie Water

Figures 4.5 and 4.6 shows the rejection of ions by the dNF-40 membrane at three cross-flow velocities (0.6 m/s, 0.75 m/s, 1 m/s) and two permeate fluxes ($20 \text{ L m}^{-2} \text{ h}^{-1}$ and $30 \text{ L m}^{-2} \text{ h}^{-1}$). The error bars indicate the standard deviation of the measurements from the mean. Rejection of sulphate was almost 100% which is similar to results obtained from the single-salt rejection tests. The rejection of Ca^{2+} was 68% and Mg^{2+} was 86%. The monovalent cations are poorly rejected due to the Donnan effect, low solvation energy and smaller radius of hydration. The rejection of monovalent anions is higher than the rejection of monovalent cations. This can be explained by the negative surface charge of the dNF-40 membrane.

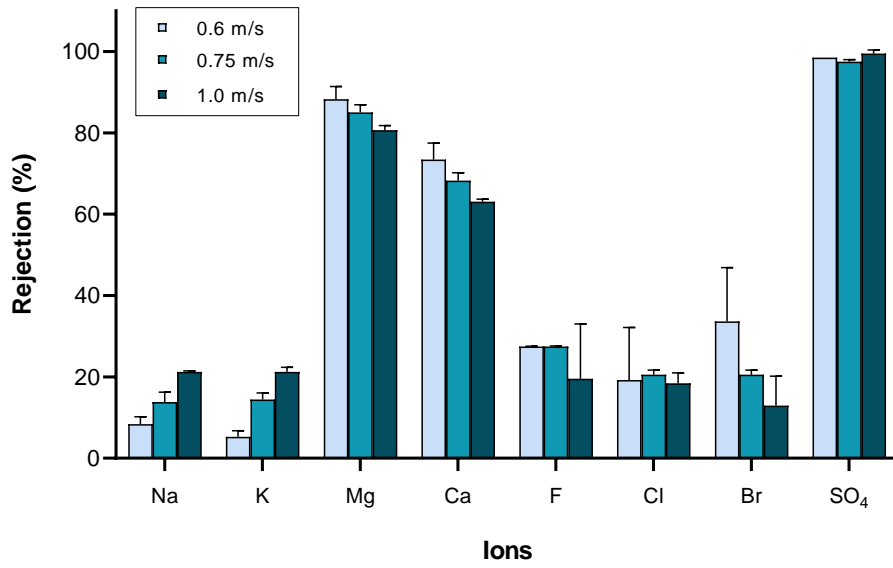


Figure 4.5: Influence of cross-flow velocity on rejection of ions in Delft Schie

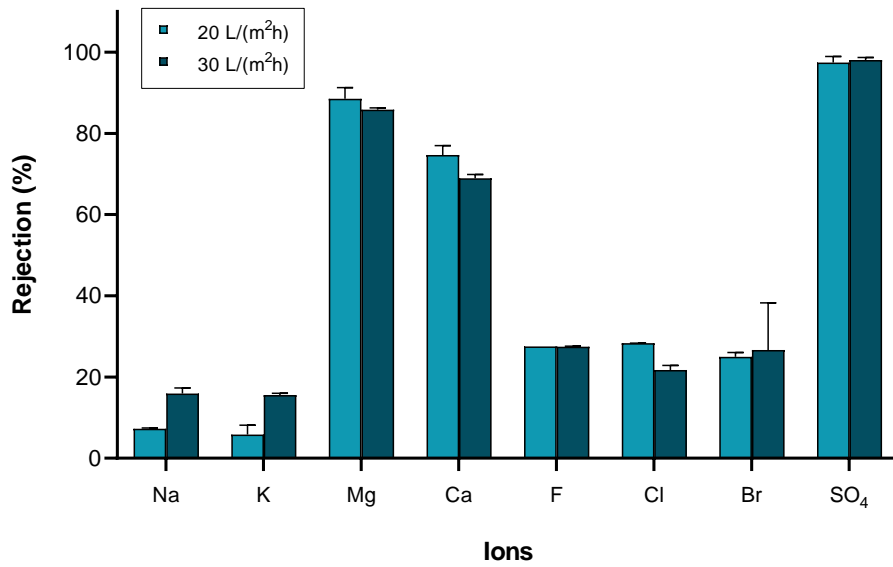


Figure 4.6: Influence of permeate flux on rejection of ions in Delft Schie

Increasing the flux increases the rejection of the monovalent cations. Rejection of Na^+ and K^+ at $30 \text{ L m}^{-2} \text{ h}^{-1}$ is almost double the rejection at $20 \text{ L m}^{-2} \text{ h}^{-1}$. This is because the increased flux causes more volume of permeate passing through the membrane and consequently, the concentration of monovalent ions in the permeate decreases. The rejection of Ca^{2+} and Mg^{2+} decreases from 85 to 80% and 72 to 62% respectively. The decrease in the rejection of divalent cations at higher fluxes can be explained by conditions of electro-neutrality as well as concentration polarization. At high fluxes, the CP factor is higher. The boundary layer at the interface is thicker at higher fluxes causing the salt to permeate through the membrane. A similar effect is observed by increasing the cross-flow velocity. This seems counter-intuitive since a higher cross-flow velocity decreases the thickness of the CP boundary layer. However, as shown in figure 4.3, the difference in the CP between cross-flow velocities 0.6 m/s and 1 m/s is not significant. The CP factor at 0.6 m/s is 1.6 and that at 1 m/s is 1.68. The increase in the rejection of the monovalent cations is due to the increase in the shear velocity of the flowing feed water through the lumen.

Figure 4.7 shows flux measured as function of time during the filtration of the Delft Schie Water. Before the test, demineralized water was circulated through the membrane and the mass transfer coefficient (MTC) was found to be around $5.83 \text{ L m}^{-2} \text{ h}^{-1} \text{ bar}^{-1}$. This was followed by filtration of the Delft Schie Water. The MTC during this phase dropped to around $5.33 \text{ L m}^{-2} \text{ h}^{-1} \text{ bar}^{-1}$. This is because of the osmotic pressure created by the solutes present in surface water. Over a period of 6 hours, no fouling was observed as the permeability remained constant. After the end of the 6-hour cycle, a demineralized water flush was conducted to flush out the surface water from system. The MTC of demineralized water was measured again. The MTC rises due to the alleviation of osmotic pressure. The average MTC after filtration was $5.78 \text{ L m}^{-2} \text{ h}^{-1} \text{ bar}^{-1}$.

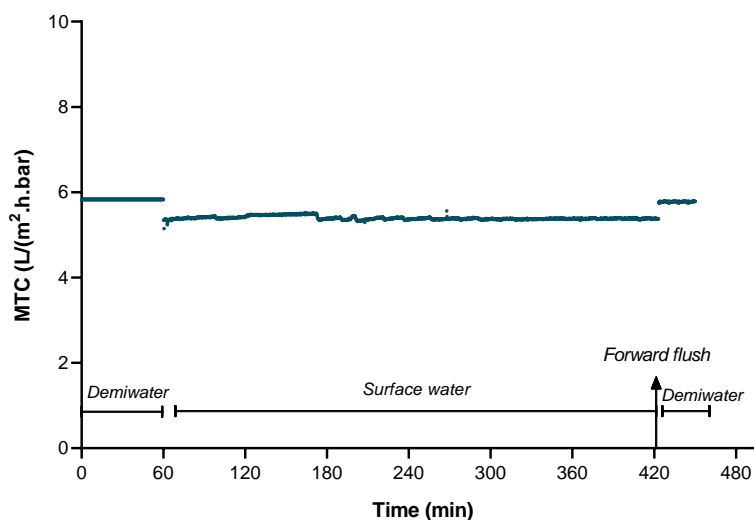


Figure 4.7: Mass transfer coefficient measurement during Schie water filtration: $V_f = 0.5 \text{ m/s}$, $J = 20 \text{ L m}^{-2} \text{ h}^{-1}$

4.5.2. Biesbosch reservoir water

The rejection and the concentration of Ca^{2+} is shown in figure 4.8. The calcium rejection remained close to 50% at recoveries of 20% and 50% i.e. a CF of 1.25 and 2 respectively. At a recovery of 80% (CF=5), the rejection increased to around 60%.

However, it is also important to assess the performance of the membrane in terms of the concentration of Ca^{2+} in the permeate since the efficiency of the treatment depends on the permeate water quality and the application of the treated water. The concentration of Ca^{2+} in the feed at 80% recovery was 126 mg/L (3.15 mmol/L) and the concentration of Ca in the permeate was around 50 mg/L (1.25 mmol/L). In order to increase water recovery, several membrane elements can be placed one after the other in series until the required recovery ratio is achieved. In such cases, the permeate from each element is collected together to obtain a single permeate stream. In this experiment, the mixed permeate roughly simulates the final permeate collected from all membrane elements at 80% recovery. In this case, the rejection is defined in terms of the mixed permeate. Samples of the mixed permeate collected during the experiments were also analysed. The mixed permeate contained 36 mg/L of Ca^{2+} which signifies a rejection of 20% with respect to the initial feed concentration. Figure 4.10 shows the influence of recovery on NOM rejection of the membrane. The rejection of NOM was unaffected by increase in recovery with respect to the initial feed concentration. A rejection of 80% was observed. Hence, the negatively charged surface plays an important role of rejecting negatively charged solutes at higher recoveries. This can also be observed in the SO_4^{2-} rejections at 80% recovery. The SO_4^{2-} rejection of 75% was observed at 80% recovery.

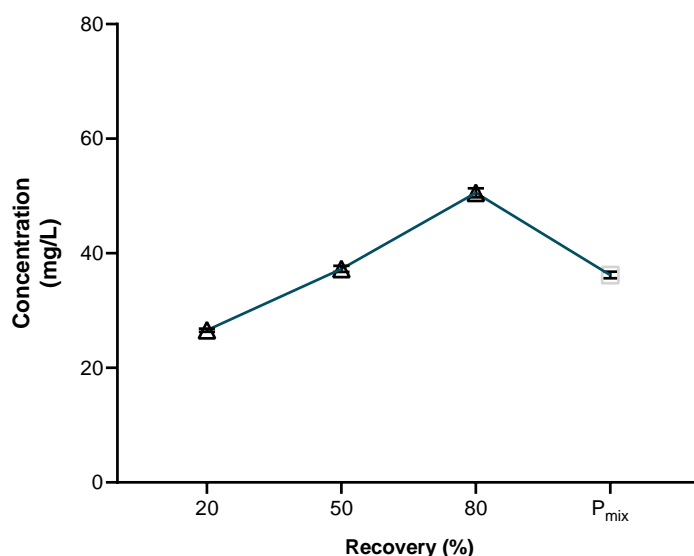


Figure 4.8: Concentration of Ca^{2+} in the permeate with at different recoveries. P_{mix} represents the mixed permeate

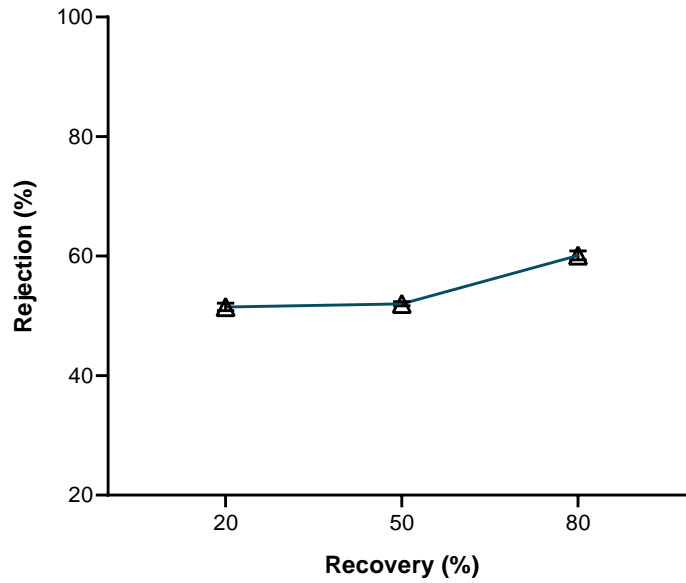


Figure 4.9: Ca²⁺ rejection with increasing recovery with respect to concentration in the feed tank

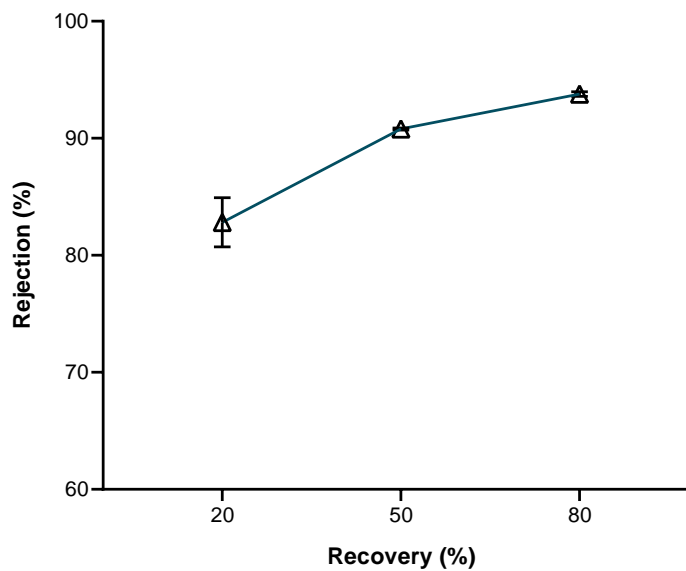


Figure 4.10: NOM rejection with increasing recovery with respect to concentration in the feed tank

A higher rejection of Ca²⁺ was observed in the Schie water than in the Biesbosch water. One possible reason for this observation could be that divalent ions such as Ca²⁺ tend to form complexes with NOM by binding with the acidic functional groups of NOM (such as carboxylic group) in the surface water which increases the size of the molecule [83]. However, the requirement for electroneutrality of the feed and permeate could have also played a role in the higher rejection of Ca²⁺ in the Schie Water.

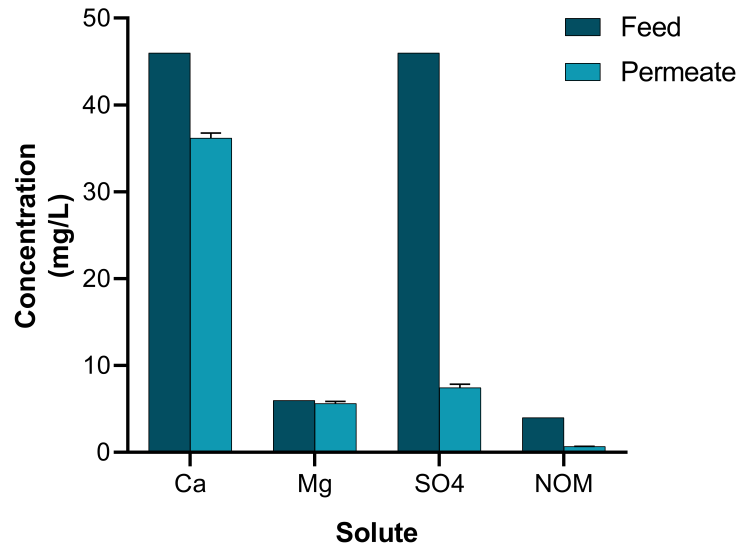


Figure 4.11: Concentration of ions and NOM in the feed and mixed permeate

4.6. Model foulant solutions

4.6.1. Sodium alginate

Figure 4.12 and 4.13 shows the flux recorded as a function of time during experiments with 100 mg/L and 200 mg/L of sodium alginate. The Ca^{2+} concentration was kept constant at 3 mM in both experiments. At the beginning of the experiment, demineralized water was circulated through the system and the MTC was measured. After 30 minutes, the demineralized water was replaced with sodium alginate solution. The flux was continuously recorded by the flow meter.

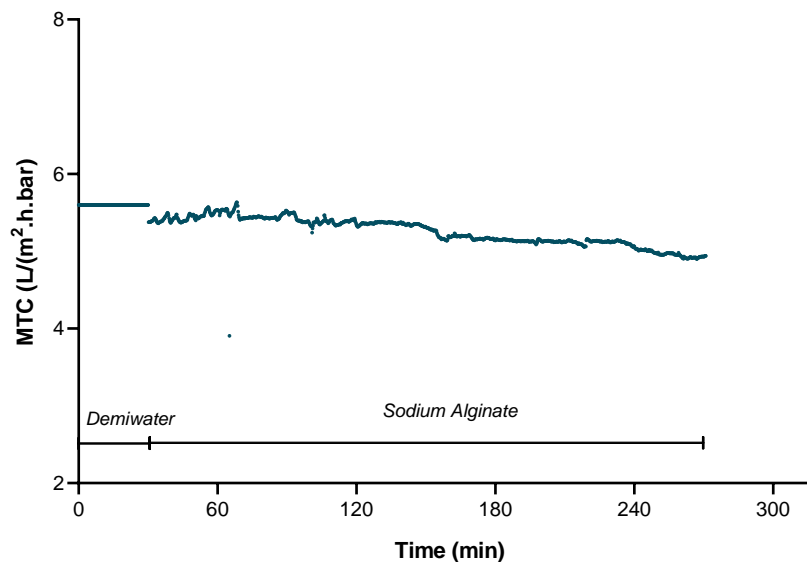


Figure 4.12: MTC measurement during sodium alginate filtration. SA=100 mg/L, Ca^{2+} =3mM

The MTC drops by around $0.2 \text{ L m}^{-2}\text{h}^{-1} \text{ bar}^{-1}$ due to osmotic pressure exerted by the solutes in the feed solution. Following the initial drop, a slow MTC decline over

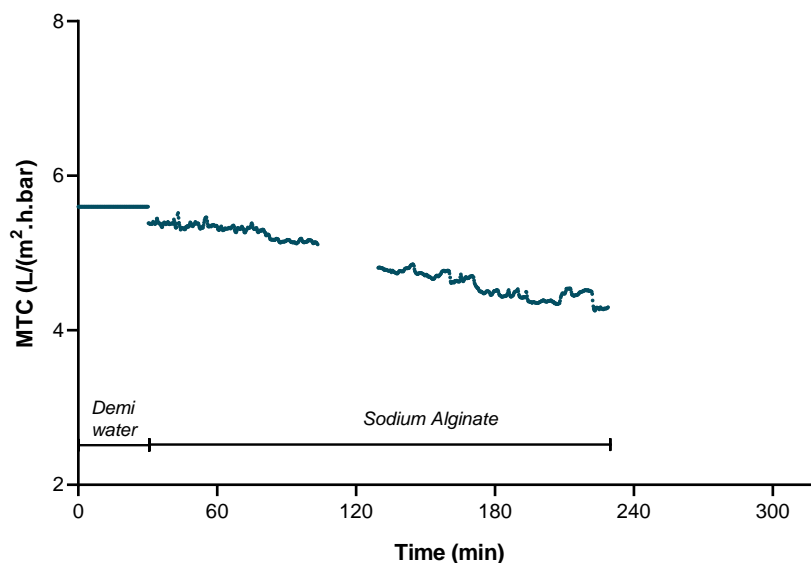


Figure 4.13: MTC measurement during sodium alginate filtration. SA=200 mg/L, Ca²⁺=3mM

time is observed over time. The MTC decline during a 4-hour filtration cycle is more severe when the alginate concentration is higher. The Ca²⁺ ions interact with the alginate to form a gel-layer which gradually covers the membrane surface. A gradual flux decline is due to the formation of an alginate gel layer on the surface of the membrane surface.

Some studies conducted in the past show that addition of calcium increases the irreversibility of the fouling [73, 84]. Irreversible fouling was caused during the tests with 200 mg/L. The pure water permeability dropped to 5.4 Lm⁻²h⁻¹bar⁻¹ and could not be restored by hydraulic flushing. Another phenomenon which was observed during the course of the experiment was the rapid rise in the differential pressure across the membrane. This was observed in all experiments with sodium alginate albeit at different rates. During the first 60 minutes, the dP increased by 125%. The possible reason for this could be blocking of the fibers by the alginate aggregates. This does not affect the flux since the incoming feed takes a low resistance along other fibers in the module at higher velocities. Another way of confirming the capillary (fibre) blocking is by measuring the forward flush pressure. During forward flushing of an unblocked membrane, no permeate is produced i.e. water does not pass across the membrane. This indicates that no pressure is applied across the membrane. However, when some percentage of the fibers are blocked, the feed-side pressure is higher than 0 bar. The forward flush pressure after a filtration cycle with 200 mg/L was 0.25 bar. In a previous study conducted by Heijman et.al. it was shown that during filtration of iron(III) hydroxide flocs, ultrafiltration capillaries were being blocked on both sides [85]. The forward flush pressure could not be removed by hydraulic flushing even at twice the filtration velocity.

Fiber blocking can occur either on the feed side or the concentrate side. Figure 4.14 shows the fiber blocking mechanism. Feed water containing the alginate aggregates enter the fibers on the feed side. The alginate molecules initially block the feed-side opening. Hydraulic flushing pushes the aggregates towards the concentrate-side opening. Fibers blocked on the capillary side cannot usually be cleaned by hydraulic flushing. Chemically Enhanced Forward Flush (CEFF) was conducted with 200 ppm

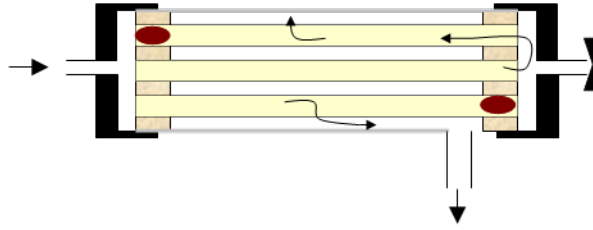


Figure 4.14: Fiber(capillary) blocking mechanism[85]

of sodium hypochlorite solution. The pH of the solution was adjusted to 11.5 using NaOH. The cleaning solution was circulated through the system for 1 hour without the production of permeate. Chemical cleaning with NaOCl was very effective in clearing out the alginate aggregates which blocked the capillaries. Chemical cleaning was able to restore the dP to 0.2 bar. The MTC measured after the cleaning was $5.83 \text{ L m}^2\text{h}^{-1} \text{ bar}^{-1}$ which is almost equal to that of the pristine membrane.

Figure 4.15 shows the effect of Ca^{2+} concentration on membrane fouling. Increasing the Ca^{2+} from 3 mM to 4 mM did not have a marked effect on the MTC decline. This result was contrary to some previous studies conducted by Jamaal et.al which showed that increasing the calcium concentration from 1.265 mM to 2.4 mM had a significant effect on the fouling of UF membranes. This could be explained by the fact that by increasing the calcium concentration, the chelating capacity is higher which causes the size of the Ca-SA aggregates to increase thus creating a porous fouling layer. The fouling layer has several pores and gaps which allow the water to pass through relatively easily.

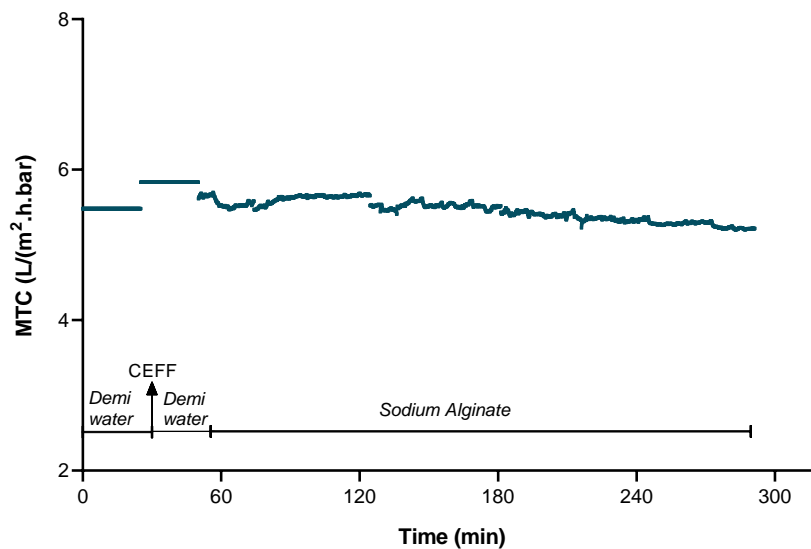


Figure 4.15: MTC measurement during sodium alginate filtration. SA=100 mg/L, Ca^{2+} =4 mM

The pH of alginate solution was changed to 4.1 to investigate the fouling properties of the membrane at low pH. The pH was adjusted using HCl. The MTC plotted as a function of time is shown in figure 4.16. The initial drop in MTC is quite severe compared to the alginate solution at pH 7 which suggests that at lower pH, the driving force for filtration decreases due to increase in membrane resistance. The MTC drops gradually over the period 4 hours. The MTC decline over 4 hours is around

14% which is significantly higher than that at pH 7 (7%). At lower pH, the zeta potential of the alginate becomes less negative which decreases the electrostatic repulsion between the membrane surface and the alginate molecules. However, the zeta potential of the alginate solution is still negative at pH 4.1 which explains why severe fouling is not observed [86]. The nature of the polyelectrolytes layers on the membrane surface also play a role in determining the severity of fouling at low pH. Strong acid functional groups such as sulfonate groups do not protonate at low pH. In contrast, weak acid functional groups such as carboxylic groups on the foulant molecule readily protonate at low pH causing the zeta potential to become more positive.

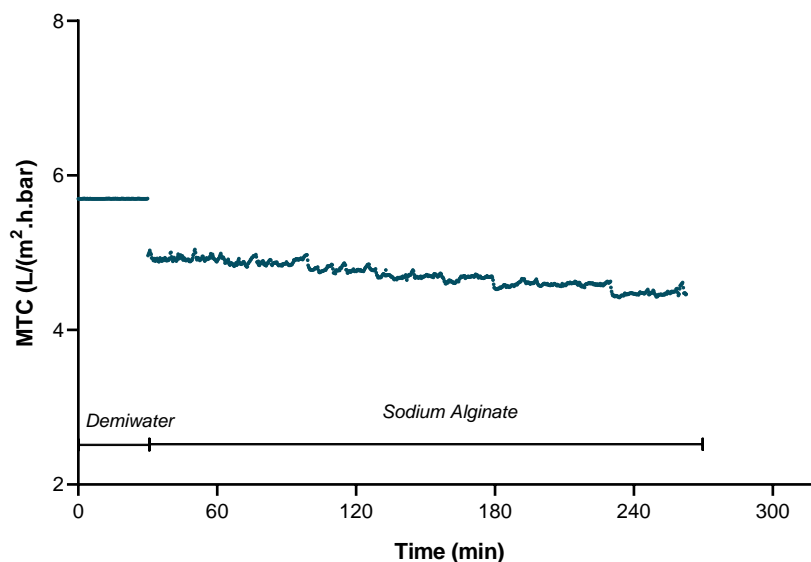


Figure 4.16: MTC measurement during sodium alginate filtration. SA=100 mg/L, Ca^{2+} =3 mM, pH=4.0

4.6.2. Humic Acid

The MTC measured as a function of time for humic acid concentrations of 10 and 20 mg/L is shown in figures 4.17 and 4.18. No flux decline was observed during humic acid filtration. The permeability remained constant throughout the duration of the tests.

Increasing the concentration of Ca^{2+} from 1mM to 3mM had no significant effect on the fouling rate. Lee and Elimelech reported that alginate (hydrophilic) fouling is much more severe than humic acid (hydrophobic) fouling because the gelation of charged macromolecules by intermolecular bridging is much more significant in alginate than in humic acid [87]. The results from the HA experiments also explain the results of the fouling experiments conducted with Delft Schie Water. Figure 4.20 shows an average LC-OCD analysis of the raw Delft Schie water. Humic substances have the highest fractional concentration in the Delft Schie, four times the amount of low MW acids. NOM in surface water is a mixture of polysaccharides and proteins (biopolymers), humic substances and low molecular weight neutrals and acids. In this experiment, humic acid was used as a surrogate for humic substances whereas alginate and BSA was used as surrogate for biopolymers. Although, biopolymers might exhibit similar fouling mechanisms, its quantity in surface water is quite low compared to humic substances. This suggests that their influence is overridden by humics which do not tend to foul this membrane under regular operating conditions.

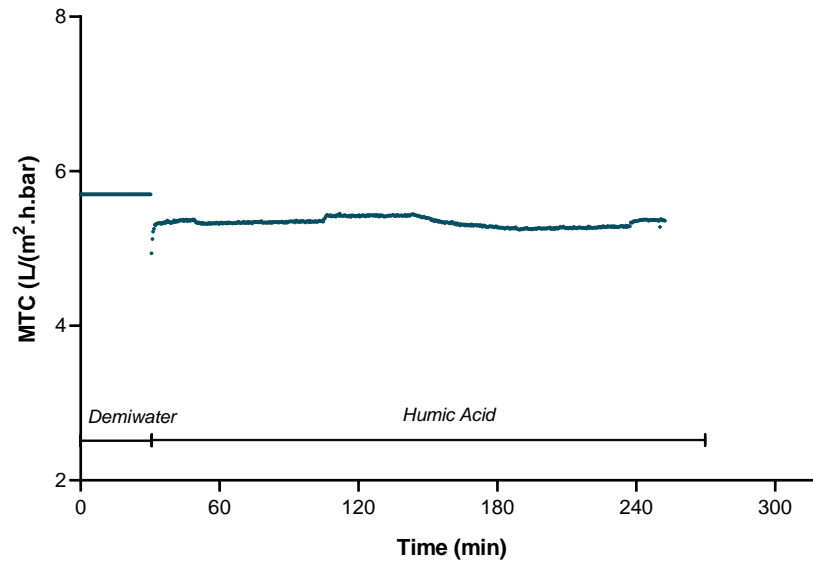


Figure 4.17: MTC measurement during humic acid filtration. HA=10 mg/L, Ca^{2+} =1 mM

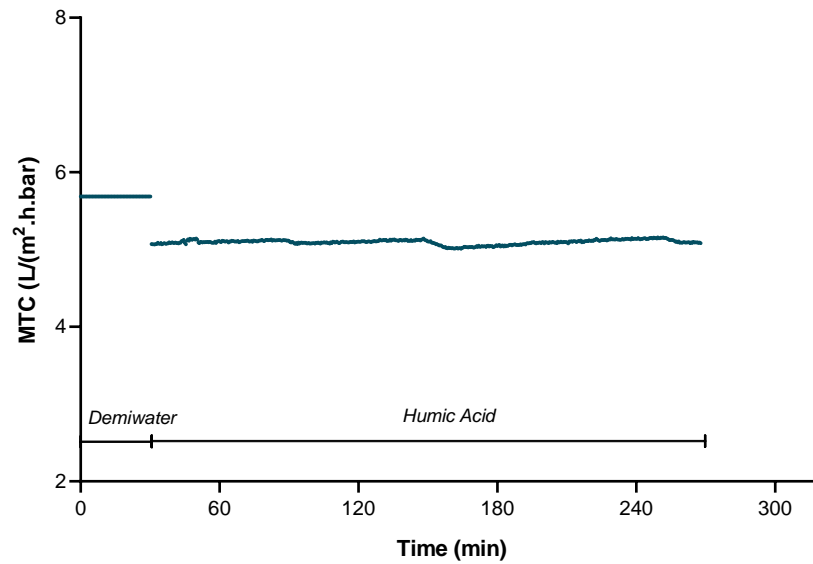


Figure 4.18: MTC measurement during humic acid filtration. HA=20 mg/L, Ca^{2+} =3 mM

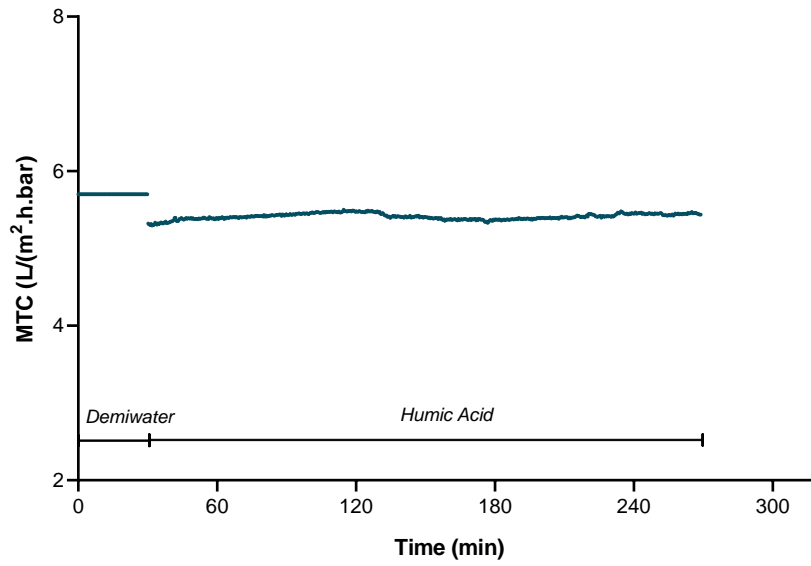


Figure 4.19: MTC measurement during humic acid filtration. HA=10 mg/L, Ca^{2+} =3 mM

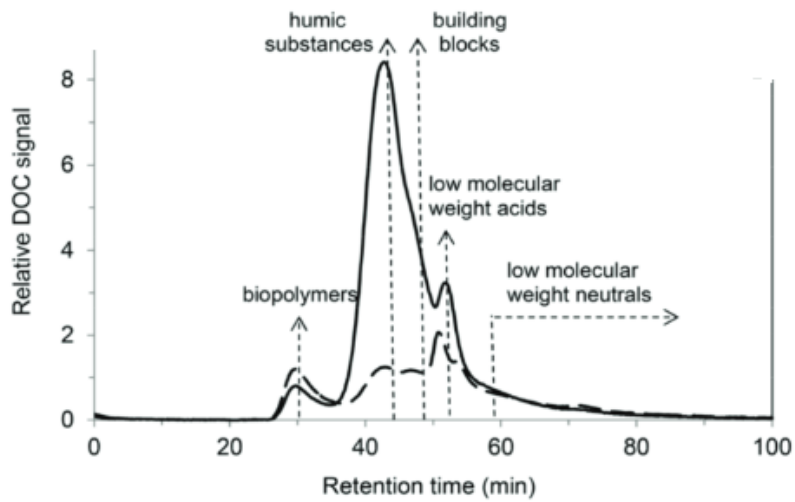


Figure 4.20: LC-OCD chromatogram of Delft Schie [88]

4.6.3. Bovine serum albumin

Membrane fouling was not observed with 20 mg/L BSA solution. The zeta potential of BSA is highly negative due to which it is strongly repelled by the membrane surface. The MTC measurement is shown in figure 4.21. He et.al. measured the flux decline in hollow fiber NF membranes using 1 g/L BSA solution and reported a flux decline of 20% over a period of 3 hours [89]. This suggests that protein fouling occurs only at higher concentrations which are not found in surface water. Another possible reason for no observed fouling during the filtration of model foulant solutions is the low surface roughness. The deposition of polyelectrolyte layers on the PES UF surface causes the surface to become smoother. A rougher membrane surface provides a larger surface area for the deposition of foulant molecules. Additionally, on a smooth surface, all the foulant molecules are subject to hydraulic shear forces in the feed channel [90]. On a rougher surface, the foulant particles trapped within the valleys are not subject to shear forces making it likely to cause fouling.

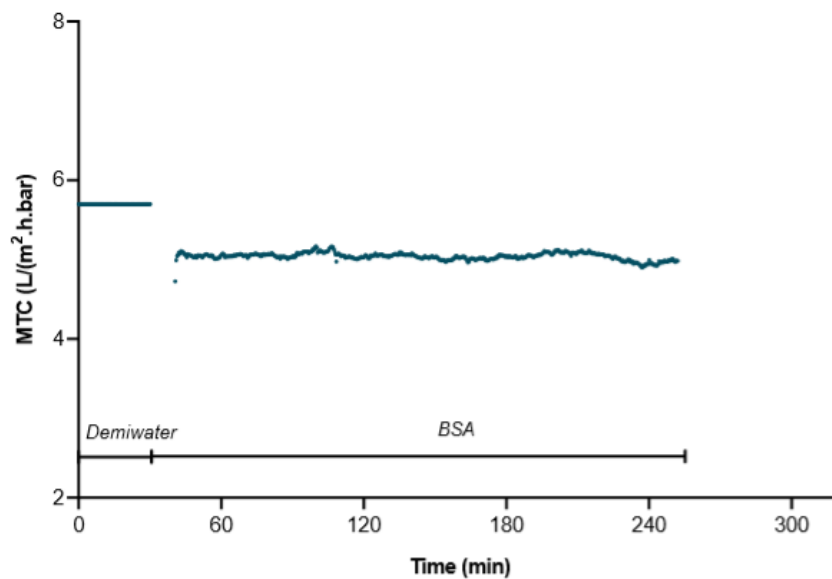


Figure 4.21: MTC measurement during humic acid filtration. BSA=20 mg/L, Ca^{2+} =3 mM

5

Conclusions and Recommendations

5.1. Conclusions

The effectiveness of the hollow fiber membrane, dNF-40 for direct nanofiltration of surface waters was determined during the study. The aim of study was to investigate the performance of the dNF-40 membrane for the direct treatment of surface water in terms of the solute rejection, fouling tendency and concentration polarization.

The rejection of Ca^{2+} was between 60-75% in Schie Water and between 50-60% in the Biesbosch water. Donnan effect is the most important rejection mechanism during filtration of surface waters. NOM present in water was well and stably rejected with final NOM concentration of less than 1 mg/L in the permeate. The rejection of NOM was around 85-90% for both surface waters.

Increasing the cross-flow velocity and the permeate flux improved the rejection of monovalent cations but decreased the rejection of Ca^{2+} and Mg^{2+} . On the other hand, the rejection of NOM was practically unaffected by changes in operational parameters. The mixed permeate at 80% recovery contained 36 mg/L of Ca^{2+} . The rejection properties of the dNF-40 membrane can be beneficial for treatment of surface water for certain applications where complete removal of hardness is not desired such as drinking water treatment. Fouling experiments were conducted with three model foulants including alginate, humic acids and BSA. No flux decline was observed during the experiments conducted with surface water. The strongly negative terminal polyelectrolyte layer repels negatively charged foulant molecules and prevents fouling. Permeability decline of 25-30% was observed with highly concentrated alginate solutions. However, it should be kept in mind that the concentrations of alginate used during the experiments were high in order to observe quicker fouling of the membranes and waters with such high concentrations of polysaccharide NOM fraction are unlikely to occur naturally. Municipal wastewater or sewage have higher concentrations of polysaccharides. The calcium in the feed water was seen to form gel-aggregates with alginate which resulted in irreversible fiber blocking. The hydraulic pressure loss was doubled in the first hour of the filtration tests. Hydraulic flushing failed to remove the alginate aggregates from the blocked fibers. Chemical cleaning with 200 ppm solution of sodium hypochlorite was conducted to alleviate fiber blocking. Other model foulants viz. humic acids and bovine serum albumin showed no membrane fouling due to their negative zeta potentials.

The limitation of this structure lies in the low permeate flux of the membrane. The membrane was observed to be vulnerable to concentration polarization at high

fluxes. The flow through hollow fibers was laminar even at very high cross-flows due to the narrow flow channel diameter. The influence of cross-flow velocity was higher at higher fluxes. The results indicated that high cross-flow velocity was required to minimize concentration polarization at high fluxes. However, a pressure drop of 0.4 bar was observed at a cross-flow velocity of 1 m/s. Although this may not be a problem for the laboratory scale membrane, the full-scale membrane module of length 1.5 metres will have a pressure drop of approximately 2 bar. Hence the application of the membrane is limited to feed waters with osmotic pressure low enough to avoid concentration polarization.

5.2. Recommendations

The results presented in this thesis demonstrate that the dNF-40 hollow fiber membrane with the LbL structure can treat surface water without pre-treatment. These membranes are ideal for drinking water treatment owing to the partial removal of hardness and complete removal of organic matter. On the basis of the conclusions, some recommendations for future research can be provided:

1. The electrical properties of the membranes were not measured during this research. Measuring the properties such as the zeta potential, surface charge density and thickness will help to provide a better understanding of rejection and fouling properties of the membrane and under which conditions, the membrane performs most efficiently.
2. The membrane should be tested for different kind of feed waters such as municipal wastewater and wastewater treatment plant effluents. Since the dNF-40 is shown to demonstrate fouling-resistant properties, treatment of wastewater with high organic matter content should be studied. Also, model foulants solutions such as alginates, humic acid and others should be investigated under different operating conditions and feed composition. Some studies have shown that adding protein to alginate solution increased the severity of fouling [73]. A similar membrane with positively charged terminal layer can be tested on waters with high concentration of heavy metals such as acid mine drainage.
3. Hydraulic forward flush and chemically enhanced forward flushing were used for membrane cleaning during this research. Hydraulic backwash as a fouling control measure can be adopted. The effect of the backwash water quality on cleaning efficiency is an interesting research. Some research has been previously conducted under the DEMIFLUSH project on capillary UF membranes [74].
4. A cost analysis can be conducted to determine under which conditions, it is beneficial to use dNF-40 membranes over spiral wound membranes. Hollow fiber membranes require a much larger cross-flow velocity to avoid concentration polarization which consumes high amount of energy. However, spiral wound membranes require pre-treatment of feed water and have a larger overall footprint. A cost analysis can be crucial in determining the best application of hollow fiber membranes
5. The dNF-40 membrane is can remove 50-70% of scale-forming ions such as Ca^{2+} and SO_4^{2-} . If further purification of water is desired (for instance, for the production of process or ultrapure water), it can be used as a first pass in a

double pass reverse osmosis. Using the low pressure dNF-40 membrane as a first pass could potentially reduce energy costs compared to an RO membrane. Additionally, the removal of salt ions such as Ca^{2+} , Mg^{2+} and SO_4^{2-} will significantly reduce the scaling potential of the water entering the second pass membrane. This would also reduce the need of chemicals such as antiscalants.

6. Over the last decade, the concentrations of organic micro-pollutants especially pharmaceutically active compounds and endocrine disrupting compounds such as diclofenac, carbamazepine and diuron have risen to unacceptable levels in natural waters. These micropollutants are notoriously difficult to remove due to their small size, varying charge properties and extremely strict quality standards. Hollow fiber Nanofiltration can be a potentially feasible option owing to its small MWCO and ability to reject charged compounds.

Bibliography

- [1] Bernt Ericsson and Gun Trägårdh. Treatment of surface water rich in humus — membrane filtration vs. conventional treatment. *Desalination*, 108(1):117 – 128, 1997. Annual Meeting of the European Desalination Society of Desalination and the Environment.
- [2] Marcel Mulder. *Basic Principles of Membrane Technology*. Springer Netherlands, 1 edition, 1991.
- [3] Shuji Nakatsuka, Ichiro Nakate, and Tadaaki Miyano. Drinking water treatment by using ultrafiltration hollow fiber membranes. *Desalination*, 106(1):55 – 61, 1996.
- [4] J.Q.J.C.Verberk. *Application of air in membrane filtration*. Phd thesis, Delft University of Technology, April 2005.
- [5] Lawrence K. Wang & Jiaping Paul Chen & Yung-Tse Hung & Nazih K. Shamas, editor. *Membrane and desalination technologies*. 2512-1359. Humana Press, 2011.
- [6] Guillo Alexander Schrader. *Direct nanofiltration of wastewater treatment plant effluent*. PhD thesis, University of Twente, Netherlands, 2006.
- [7] Z.F. Cui, Y. Jiang, and R.W. Field. Chapter 1 - fundamentals of pressure-driven membrane separation processes. In Z.F. Cui and H.S. Muralidhara, editors, *Membrane Technology*, pages 1 – 18. Butterworth-Heinemann, Oxford, 2010.
- [8] M.J.W. Frank, M.J.W. Frank, G. Bargeman, A. Zwijnenburg, and Matthias Wessling. Capillary hollow fiber nanofiltration membranes. *Separation and purification technology*, 22(23):499–506, 2001.
- [9] Chang Liu, Lei Shi, and Rong Wang. Enhanced hollow fiber membrane performance via semi-dynamic layer-by-layer polyelectrolyte inner surface deposition for nanofiltration and forward osmosis applications. *Reactive and Functional Polymers*, 86:154 – 160, 2015.
- [10] Shazia Ilyas, Renee English, Pierre Aimar, Jean-François Lahitte, and Wiebe M. de Vos. Preparation of multifunctional hollow fiber nanofiltration membranes by dynamic assembly of weak polyelectrolyte multilayers. *Colloids and Surfaces A: Physicochemical and Engineering Aspects*, 533:286 – 295, 2017.
- [11] <https://www.toyobo-global.com/seihin/ro/tokucho.htm>. Toyobo water treatment membranes (reverse osmosis membrane element), 2006.
- [12] Harry Futselaar, Henk Schonewille, and Walter van der Meer. Direct capillary nanofiltration for surface water. *Desalination*, 157(1):135 – 136, 2003. Desalination and the Environment: Fresh Water for all.

- [13] Gongduan Fan, Zhaoyue Su, Rujing Lin, Xiuyong Lin, Renxin Xu, and Wei Chen. Influence of membrane materials and operational modes on the performance of ultrafiltration modules for drinking water treatment. *International Journal of Polymer Science*, 2016:1–8, 03 2016.
- [14] <https://synderfiltration.com/learning-center/articles/module-configurations-process/hollow-fiber-membranes/>. Synder filtration.
- [15] Maryam Homayoonfal, Ahmad Akbari, and Mohammad Reza Mehrnia. Preparation of polysulfone nanofiltration membranes by uv-assisted grafting polymerization for water softening. *Desalination*, 263(1):217 – 225, 2010.
- [16] Yulong Ying, Wen Ying, Qiaochu Li, Donghui Meng, Guohua Ren, Rongxin Yan, and Xinsheng Peng. Recent advances of nanomaterial-based membrane for water purification. *Applied Materials Today*, 7:144 – 158, 2017.
- [17] Omar Labban, Tzyy Chong, and Lienhard V. Design and modeling of novel low-pressure nanofiltration hollow fiber modules for water softening and desalination pretreatment. *Desalination*, 439:58–72, 08 2018.
- [18] Daniel Menne, Matthias Wessling, and Nieck E Benes. Layer-by-layer design of nanofiltration membranes. 2017.
- [19] Yan Liu, George Chen, Xiuli Yang, and Huining Deng. Preparation of layer-by-layer nanofiltration membranes by dynamic deposition and crosslinking. *Membranes*, 9:20, 01 2019.
- [20] Chang Liu. Development of novel layer-by-layer assembled nanofiltration hollow fiber membranes for water treatment. 2015.
- [21] Chang Liu, Lei Shi, and Rong Wang. Crosslinked layer-by-layer polyelectrolyte nanofiltration hollow fiber membrane for low-pressure water softening with the presence of SO_4^{2-} in feed water. *Journal of Membrane Science*, 486:169 – 176, 2015.
- [22] Nithya Joseph, Pejman Ahmadiannamini, and Hoogenboom Richard. Layer-by-layer preparation of polyelectrolyte multilayer membranes for separation. *Polymer Chemistry*, 01 2013.
- [23] Elizabeth Arkhangelsky, Denis Kuzmenko, and Vitaly Gitis. Impact of chemical cleaning on properties and functioning of polyethersulfone membranes. *Journal of Membrane Science*, 305(1):176 – 184, 2007.
- [24] Lawrence Dresner. Some remarks on the integration of the extended nernst-planck equations in the hyperfiltration of multicomponent solutions. *Desalination*, 10(1):27 – 46, 1972.
- [25] R. Schlögl. Membrane permeation in systems far from equilibrium. *Berichte der Bunsengesellschaft für physikalische Chemie*, 70(4):400–414, 1966.
- [26] Oluranti Agboola, J.P. Maree, Andrei Kolesnikov, kadiambuji kady Mbaya, and Rotimi Sadiku. Theoretical performance of nanofiltration membranes for wastewater treatment. *Environmental Chemistry Letters*, 13, 03 2015.

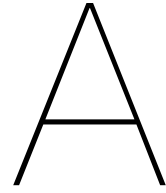
- [27] Omar Labban, Chang Liu, Tzyy Haur Chong, and John H Lienhard. Fundamentals of low-pressure nanofiltration: Membrane characterization, modeling, and understanding the multi-ionic interactions in water softening. 2017.
- [28] Bart Van der Bruggen. *Nanofiltration*, pages 1–23. American Cancer Society, 2013.
- [29] Ran Shang, Aristeidis Goulas, Chuyang Y. Tang, Xavier de Frias Serra, Luuk C. Rietveld, and Sebastiaan G.J. Heijman. Atmospheric pressure atomic layer deposition for tight ceramic nanofiltration membranes: Synthesis and application in water purification. *Journal of Membrane Science*, 528:163 – 170, 2017.
- [30] D. Diamantidou. Ionic separation of the iex spent regenerant using nanofiltration. mathesis, Delft University of Technology, 2018.
- [31] Frederick George Donnan. Theory of membrane equilibria and membrane potentials in the presence of non-dialysing electrolytes. a contribution to physical-chemical physiology. *Journal of Membrane Science*, 100(1):45 – 55, 1995. The early history of membrane science selected papers celebrating vol. 100.
- [32] Patrick Fievet. *Donnan Effect*, pages 1–3. Springer Berlin Heidelberg, Berlin, Heidelberg, 2015.
- [33] Phuong Tu Nguyen. Role of charge effects during membrane filtration. mathesis, Ghent University, 2013.
- [34] Soo-Jin Park and Min-Kang Seo. Chapter 1 - intermolecular force. In Soo-Jin Park and Min-Kang Seo, editors, *Interface Science and Composites*, volume 18 of *Interface Science and Technology*, pages 1 – 57. Elsevier, 2011.
- [35] U. Beck U. van Rienen E. Gongadze, S. Petersen. Classical models of the interface between an electrode and an electrolyte. In *COMSOL*, 2009.
- [36] Ran Shang. Ceramic ultra- and nanofiltration for municipal wastewater reuse. 2014.
- [37] A. Yaroschuk. Rejection mechanisms of nf membranes. *Membrane Technology*, 1998(100):9 – 12, 1998.
- [38] W.Richard Bowen and Julian Welfoot. Modelling the performance of membrane nanofiltration—critical assesment and model development. *Chemical Engineering Science*, 57:1121–1137, 04 2002.
- [39] Berrin Tansel, John Sager, Tony Rector, Jay Garland, Richard F. Strayer, Lanfang Levine, Michael Roberts, Mary Hummerick, and Jan Bauer. Significance of hydrated radius and hydration shells on ionic permeability during nanofiltration in dead end and cross flow modes. *Separation and Purification Technology*, 51:40–47, 2006.
- [40] Anthony G. Fane. Ultrafiltration: factors influencing flux and rejection. 1986.
- [41] Genick Bar-Meir. *Basics of Fluid Mechanics*. University Press of Florida, 2009.
- [42] Glenn Brown. The history of the darcy-weisbach equation for pipe flow resistance. *Proc. Environ. Water Resour. Hist.*, 38, 10 2002.

- [43] J. S. Vrouwenvelder, C. Hinrichs, W. G.J. Van der Meer, M. C.M. Van Loosdrecht, and J. C. Kruithof. Pressure drop increase by biofilm accumulation in spiral wound ro and nf membrane systems: role of substrate concentration, flow velocity, substrate load and flow direction. *Biofouling*, 25(6):543–555, 2009. PMID: 19437193.
- [44] Anh H. Nguyen, John E. Tobiasson, and Kerry J. Howe. Fouling indices for low pressure hollow fiber membrane performance assessment. *Water Research*, 45(8):2627 – 2637, 2011.
- [45] A.I. Schäfer, A. Pihlajamäki, A.G. Fane, T.D. Waite, and M. Nyström. Natural organic matter removal by nanofiltration: effects of solution chemistry on retention of low molar mass acids versus bulk organic matter. *Journal of Membrane Science*, 242(1):73 – 85, 2004. Membrane Engineering Special Issue.
- [46] Eiji Iritani and Nobuyuki Katagiri. Developments of blocking filtration model in membrane filtration. *KONA Powder and Particle Journal*, 33:179–202, 2016.
- [47] Thang Nguyen, Felicity Roddick, and Linhua Fan. Biofouling of water treatment membranes: A review of the underlying causes, monitoring techniques and control measures. *Membranes*, 2:804–40, 12 2012.
- [48] Andreas Broeckmann, Thomas Wintgens, and Andrea Iris Schäfer. Removal and fouling mechanisms in nanofiltration of polysaccharide solutions. 2005.
- [49] Joerg Winter, Benoit Barbeau, and Pierre Berube. Nanofiltration and tight ultrafiltration membranes for natural organic matter removal—contribution of fouling and concentration polarization to filtration resistance. *Membranes*, 7:34, 07 2017.
- [50] A.I. Schäfer, A.G. Fane, and T.D. Waite. Nanofiltration of natural organic matter: Removal, fouling and the influence of multivalent ions. *Desalination*, 118(1):109 – 122, 1998. Conference Membranes in Drinking and Industrial Water Production.
- [51] Sébastien Déon, Patrick Dutournié, Patrick Fievet, Lionel Limousy, and Patrick Bourseau. Concentration polarization phenomenon during the nanofiltration of multi-ionic solutions: Influence of the filtrated solution and operating conditions. *Water Research*, 47(7):2260 – 2272, 2013.
- [52] S. Bhattacharjee. Concentration polarization: Early theories. Technical report, Water Planet, Inc., 2017.
- [53] J. P. van der Hoek L. Rietveld B. Heijman D. van Halem, W. van der Meer and M. Keuten. *Nanofiltration Lab Experiments*. Delft University of Technology, 2009.
- [54] Richard W. Baker. *Membrane Technology and Applications, Second Edition*. John Wiley & Sons, Ltd, March 2004.
- [55] Sirshendu De and P.K Bhattacharya. Mass transfer coefficient with suction including property variations in applications of cross-flow ultrafiltration. *Separation and Purification Technology*, 16(1):61 – 73, 1999.

- [56] Alexandre Giacobbo, Andréa Bernardes, Maria Rosa, and Maria Pinho. Concentration polarization in ultrafiltration/nanofiltration for the recovery of polyphenols from winery wastewaters. *Membranes*, 8:46, 07 2018.
- [57] Munir Cheryan. *Ultrafiltration and microfiltration: handbook*. CRC Press, 2010.
- [58] G.B. van den Berg, I.G. Racz, and C.A. Smolders. Mass transfer coefficients in cross-flow ultrafiltration. *Journal of membrane science*, 47(1-2):25–51, 1989.
- [59] G. Schock and A. Miquel. Mass transfer and pressure loss in spiral wound modules. *Desalination*, 64:339 – 352, 1987.
- [60] A. Pérez-González, R. Ibáñez, P. Gómez, A.M. Urriaga, I. Ortiz, and J.A. Irabien. Nanofiltration separation of polyvalent and monovalent anions in desalination brines. *Journal of Membrane Science*, 473:16 – 27, 2015.
- [61] H.M. Krieg, S.J. Modise, K. Keizer, and H.W.J.P. Neomagus. Salt rejection in nanofiltration for single and binary salt mixtures in view of sulphate removal. *Desalination*, 171(2):205 – 215, 2005.
- [62] Dipankar Nanda, Kuo-Lun Tung, Yu-Ling Li, Nien-Jung Lin, and Ching-Jung Chuang. Effect of pH on membrane morphology, fouling potential, and filtration performance of nanofiltration membrane for water softening. *Journal of Membrane Science*, 349:411–420, 03 2010.
- [63] Yagnaseni Roy, David M. Warsinger, and John H. Lienhard. Effect of temperature on ion transport in nanofiltration membranes: Diffusion, convection and electromigration. *Desalination*, 420:241 – 257, 2017.
- [64] Izzati Yusoff, Rosiah Rohani, and Abdul Mohammad. Molecular weight cut-off determination of pressure filtration membranes via colorimetric detection method. *Malaysian Journal of Analytical Sciences*, 21:484–495, 04 2017.
- [65] Harmen Jan Zwijnenberg, S.M. Dutczak, M.E. Boerrigter, Mark A. Hempenius, Maria W.J. Luiten-Olieman, Nieck Edwin Benes, Matthias Wessling, and Dimitrios Stamatialis. Important factors influencing molecular weight cut-off determination of membranes in organic solvents. *Journal of membrane science*, 390-391:211–217, 2012.
- [66] Bart Van der Bruggen and Carlo Vandecasteele. Modelling the retention of uncharged molecules with nanofiltration. *Water research*, 36:1360–8, 04 2002.
- [67] S Singh, K.C Khulbe, T Matsuura, and P Ramamurthy. Membrane characterization by solute transport and atomic force microscopy. *Journal of Membrane Science*, 142(1):111 – 127, 1998.
- [68] W.R. Bowen and A.W. Mohammad. Characterization and prediction of nanofiltration membrane performance—a general assessment. *Chemical Engineering Research and Design*, 76(8):885 – 893, 1998. Separation Processes.
- [69] Hisham T. El-Dessouky and Hisham M. Ettouney. Chapter 7 - reverse osmosis. In Hisham T. El-Dessouky and Hisham M. Ettouney, editors, *Fundamentals of Salt Water Desalination*, pages 409 – 437. Elsevier Science B.V., Amsterdam, 2002.

- [70] Sondus Jamal, Sheng Chang, and Hongde Zhou. Filtration behaviour and fouling mechanisms of polysaccharides. *Membranes*, 4(3):319–332, 2014.
- [71] Shujuan Meng and Yu Liu. Alginate block fractions and their effects on membrane fouling. *Water Research*, 47(17):6618 – 6627, 2013.
- [72] Amine Charfi, Hoseok Jang, and Jeonghwan Kim. Membrane fouling by sodium alginate in high salinity conditions to simulate biofouling during seawater desalination. *Bioresource Technology*, 240:106 – 114, 2017. Special issue on Challenges in Environmental Science and Engineering, CESE-2016.
- [73] S. Jamal, S. Chang, and H. Zhou. Filtration behaviour and fouling mechanisms of polysaccharides. *Membranes (Basel)*, 4(3):319–32, 2014.
- [74] Shuiqing Li. A new concept of ultrafiltration fouling control: Backwashing with low ionic strength water. 2011.
- [75] W.J.C. van de Ven, K. van't Sant, I.G.M. Pünt, A. Zwijnenburg, A.J.B. Kemperman, W.G.J. van der Meer, and M. Wessling. Hollow fiber dead-end ultrafiltration: Influence of ionic environment on filtration of alginates. *Journal of Membrane Science*, 308(1):218 – 229, 2008.
- [76] Chuyang Y. Tang, Young-Nam Kwon, and James O. Leckie. Fouling of reverse osmosis and nanofiltration membranes by humic acid—effects of solution composition and hydrodynamic conditions. *Journal of Membrane Science*, 290(1):86 – 94, 2007.
- [77] Mohammad Ali Zazouli, Simin Nasser, and Mathias Ulbricht. Fouling effects of humic and alginic acids in nanofiltration and influence of solution composition. *Desalination*, 250(2):688 – 692, 2010.
- [78] Sean T. Kelly and Andrew L. Zydney. Effects of intermolecular thiol–disulfide interchange reactions on bsa fouling during microfiltration. *Biotechnology and Bioengineering*, 44(8):972–982, 1994.
- [79] Tatsuo Maruyama, Shinji Katoh, Mitsutoshi Nakajima, and Hiroshi Nabetani. Mechanism of bovine serum albumin aggregation during ultrafiltration. *Biotechnology and Bioengineering*, 75(2):233–238, 2001.
- [80] A. Arun;S. Flambouris. Investigating the effect of operational flux and solution compositions on mwco measurements for polyamide nanofiltration membranes. TU Delft, 2018.
- [81] Shin ichi Nakao. Determination of pore size and pore size distribution: 3. filtration membranes. *Journal of Membrane Science*, 96(1):131 – 165, 1994.
- [82] Herbert S. Harned and Robert M. Hudson. The diffusion coefficient of magnesium sulfate in dilute aqueous solution at 25°. *Journal of the American Chemical Society*, 73(12):5880–5882, 1951.
- [83] Won-Young Ahn, Andrey G. Kalinichev, and Mark M. Clark. Effects of background cations on the fouling of polyethersulfone membranes by natural organic matter: Experimental and molecular modeling study. *Journal of Membrane Science*, 309(1):128 – 140, 2008.

- [84] K. Katsoufidou, S.G. Yiantsios, and A.J. Karabelas. An experimental study of uf membrane fouling by humic acid and sodium alginate solutions: the effect of backwashing on flux recovery. *Desalination*, 220(1):214 – 227, 2008. European Desalination Society and Center for Research and Technology Hellas (CERTH), Sani Resort 22 –25 April 2007, Halkidiki, Greece.
- [85] SGJ Heijman, M Vantieghem, S Raktoc, JQJC Verberk, and JC van Dijk. Blocking of capillaries as fouling mechanism for dead-end operated ultrafiltration membranes. In *Proceedings of the AMTA-Conference*, pages 1–8. s.n., 2004.
- [86] Zipei Zhang, Ruojie Zhang, Liqiang Zou, and David Julian McClements. Protein encapsulation in alginate hydrogel beads: Effect of ph on microgel stability, protein retention and protein release. *Food Hydrocolloids*, 58:308 – 315, 2016.
- [87] Sangyoun Lee and Menachem Elimelech. Relating organic fouling of reverse osmosis membranes to intermolecular adhesion forces. *Environmental Science & Technology*, 40(3):980–987, 2006. PMID: 16509346.
- [88] Hu. Jingyi. *Micro-pollutant removal from wastewater treatment plant effluent by activated carbon*. PhD thesis, Delft University of Technology, 2016.
- [89] Yuantao He, Jing Miao, Zhibin Jiang, Kai Tu, Hao Yang, Shunquan Chen, Ling Zhang, and Rui Zhang. Improving the anti-fouling property and permeate flux of hollow fiber composite nanofiltration membrane using β -cyclodextrin. *Scientific Reports*, 9(1):12435, 2019.
- [90] Qilin Li, Zhihua Xu, and Ingo Pinnau. Fouling of reverse osmosis membranes by biopolymers in wastewater secondary effluent: Role of membrane surface properties and initial permeate flux. *Journal of Membrane Science*, 290(1):173 – 181, 2007.



MTC Measurement of Biesbosch water

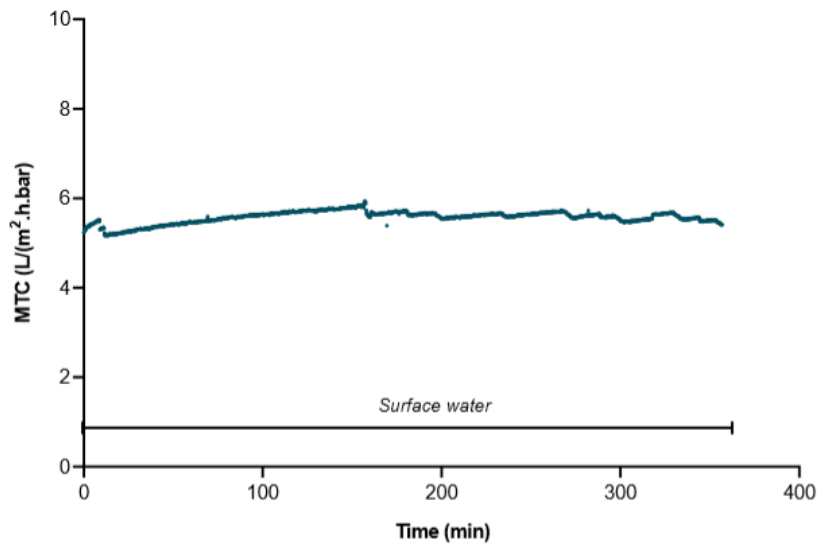


Figure A.1: Mass transfer coefficient measurement during Biesbosch water filtration: CFV= 0.5 m/s

B

Rejection of ions present in Biesbosch water

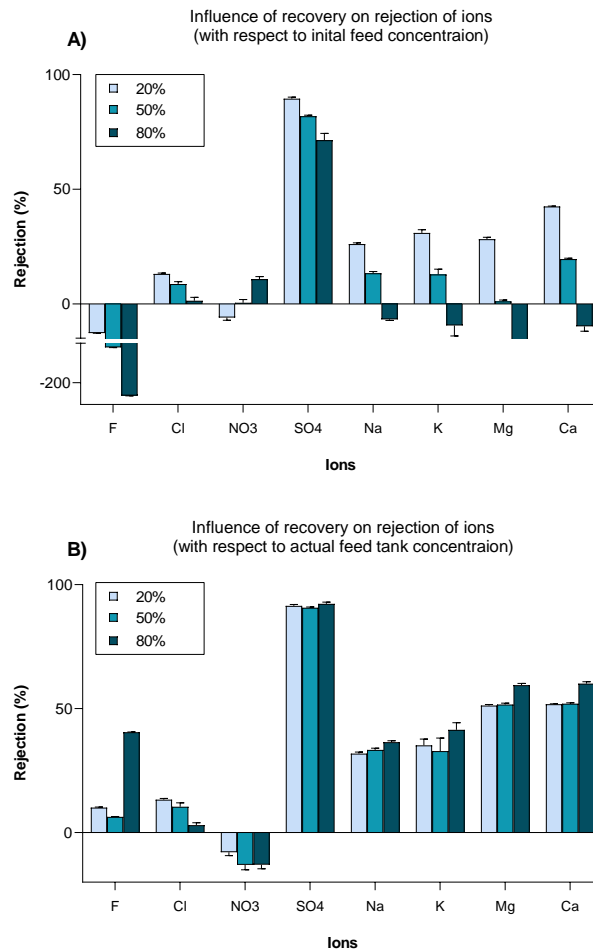
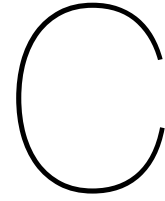


Figure B.1: Rejection of ions in Biesbosch water with respect to A) initial feed concentration and B) actual concentration of ion in the feed tank



Concentration polarization during PEG experiment

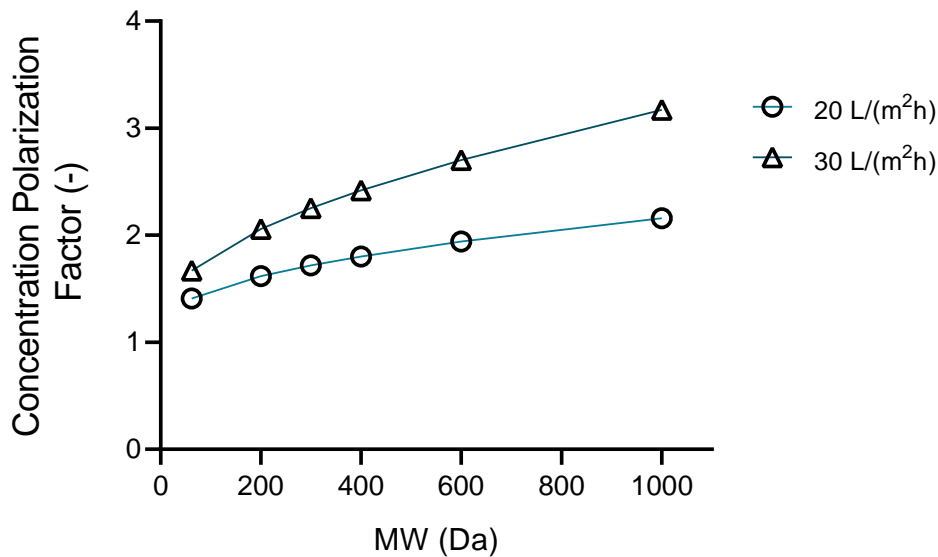


Figure C.1: Concentration polarization factors of different PEG MW fractions

The diffusion coefficients of PEG molecules were calculated using Stokes equation shown in equation C.1. Table C.1 shows the diffusion coefficients of different PEG fractions.

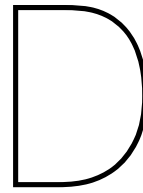
$$D = \frac{kT}{6\pi\mu r_p} \quad (\text{C.1})$$

where r_p is the Stokes radius of the PEG molecule given by

$$r_p = 0.0325(MW)^{0.437} \quad (\text{C.2})$$

Table C.1: Diffusion coefficients of PEG molecules

MW (Da)	Stokes radius (nm)	Diffusion coefficient (m ² /s)
62	0.197	1.18×10^{-9}
200	0.329	7.11×10^{-10}
300	0.393	5.96×10^{-10}
400	0.445	5.25×10^{-10}
600	0.532	4.40×10^{-10}
1000	0.665	3.52×10^{-10}



Rejection of NOM in Schie Water

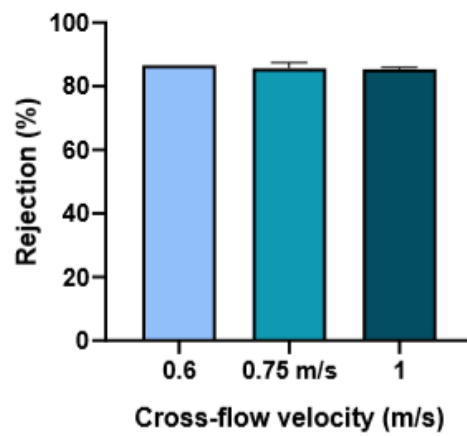


Figure D.1: Influence of cross-flow velocity on rejection of NOM in Schie Water

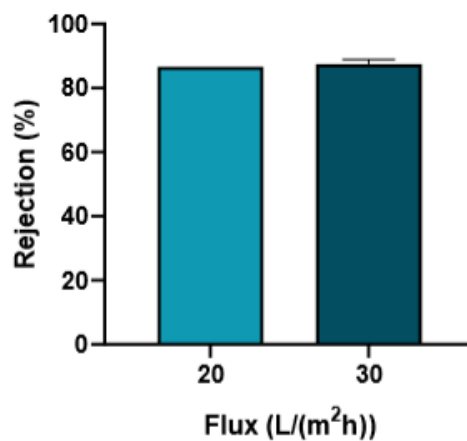


Figure D.2: Influence of flux on rejection of NOM in Schie Water